Two RNA-binding proteins mediate the sorting of miR223 from mitochondria into exosomes

Liang Ma[1], Jasleen Singh[1], and Randy Schekman[1 *]

[1]Department of Molecular and Cell Biology, Howard Hughes Medical Institute, University of California, Berkeley, United States.

[*]For correspondence: schekman@berkeley.edu

Abstract

Fusion of multivesicular bodies (MVBs) with the plasma membrane results in the secretion of intraluminal vesicles (ILVs), or exosomes. The sorting of one exosomal cargo RNA, miR223, is facilitated by the RNA-binding protein, YBX1 (Shurtleff et al., 2016). We found that miR223 specifically binds a “cold shock" domain (CSD) of YBX1 through a 5’ proximal sorting motif UCAGU. Prior to sorting into exosomes, most of the cytoplasmic miR223 resides in mitochondria. An RNA-binding protein localized to the mitochondrial matrix, YBAP1, appears to serve as a negative regulator of miR223 enrichment into exosomes. miR223 levels decreased in the mitochondria and increased in exosomes after loss of YBAP1. We observed YBX1 shuttle between mitochondria and endosomes in live cells. YBX1 also partitions into P body granules in the cytoplasm (Liu et al., 2021). We propose a model in which miR223 and likely other miRNAs are stored in mitochondria and are then mobilized by YBX1 to cytoplasmic phase condensate granules for capture into invaginations in the endosome that give rise to exosomes.

Introduction

Extracellular vesicles (EVs) bud from the plasma membrane or are secreted when multivesicular bodies (MVB) fuse with the plasma membrane to release a population of vesicles called exosomes. EVs and their cargos are highly dependent on their membrane source. Microvesicles

released by budding from the plasma membrane are a heterogeneous population of EVs ranging in size from 30 nm to 1000 nm (Cocucci et al., 2009). Exosomes are 30 nm to 150 nm in size and originate as vesicles invaginated into the interior of an MVB to form intraluminal vesicles (ILVs) (Harding et al., 1983).

Many RNAs are selectively sorted into EVs, especially small RNAs. Several studies have indicated that RNA binding proteins (RNPs) may be involved in the enrichment of RNAs into EVs (Mukherjee et al., 2016; Santangelo et al., 2016; Teng et al., 2017; Villarroya-Beltri et al., 2013). However, many of these studies used sedimentation at ~100,000 g to collect EVs, which may also collect RNP particles not enclosed within membranes which complicates the interpretation of these data. To address this question, we previously developed buoyant density-based methods separate EVs from non-vesicular aggregates and found that EVs form two distinct populations of high and low buoyant density (Shurtleff *et al.*, 2016; Temoche-Diaz et al., 2020) . We found that some miRNAs are selectively enriched in a high buoyant density vesicle fraction characterized by an enrichment in the exosomal marker protein CD63, whereas the low buoyant density EVs are fairly non-selective in the capture of miRNAs (Temoche-Diaz et al., 2019). We developed a cell-free reaction to identify YBX1 as required for miR223 sorting into exosomes and demonstrated that it plays an important role in the enrichment of miR223 into exosomes in HEK293T cells (Shurtleff *et al.*, 2016). We subsequently found that phase separated YBX1 condensates selectively recruit miR223 in vitro and sort it into exosomes in cells (Liu *et al.*, 2021). In this study we report that YBX1 directly and specifically binds miR223 by its “cold shock” domain (CSD). We have identified a positive

sorting motif, UCAGU, in miR223 for sorting into exosomes. We also found a significant fraction of cytoplasmic miR223 localized within mitochondria, tightly associated with the mitochondrial envelope and that a mitochondrial RNA-binding protein, YBAP1, may control the transfer of miR223 from mitochondria to exosomes.

Results

YBX1 directly and specifically binds miR223

We previously documented that YBX1 facilitates miR223 sorting into exosomes (Shurtleff *et al.*, 2016) and that exosomal miR223 is decreased in YBX1 knockout cells (Liu *et al.*, 2021). We reexamined the enrichment and confirmed that exosomal miR223 was decreased in exosomes purified from YBX1 KO cells (Figure 1a).

Whereas the importance of YBX1 for miR223 sorting has been established, the mechanism of their interaction was not known. To examine the direct interaction of YBX1 and miR223, we used an electrophoretic mobility shift assay (EMSA) with purified recombinant YBX1, expressed in insect cells (Figure 1 supplement 1a), and chemically synthetic miR223 and miR190, a cytoplasmic miRNA that is not enriched in exosomes. Purified YBX1 was titrated and incubated with 5' fluorescently labeled miR223 at 30℃ for 30min. miR223-YBX1 complexes were separated by electrophoresis and detected by in-gel fluorescence. The EMSA data showed that YBX1 directly and specifically bound to miR223 but ~50-fold less well with miR190 (Figure 1b-c). The measured Kd for YBX1:miR223 was 5.3nM (Figure 1d).

97 YBX1 has three major domains including an N-terminal alanine/proline-rich
98 (A/P) domain, a central cold shock domain (CSD) and a C-terminal domain
99 (CTD) (Figure 1e). To explore which specific domain of YBX1 binds
100 miR223, we constructed a series of fragments: the A/P domain, CSD and
101 CTD (Figure 1f). The YBX1 fragments were expressed in and purified from
102 insect cells (Figure 1 supplement 1b). EMSA data showed that the A/P
103 domain and CTD had little or no affinity for miR223, whereas the CSD
104 domain retained some binding affinity but not as much as full length YBX1.
105 We then constructed two combined fragments of the A/P and CSD and
106 CSD and CTD domains (Figure 1 supplement 1c). The EMSA data
107 showed that the A/P domain was dispensable and the CSD plus CTD
108 bound miR223 comparable to full length of YBX1 (Figure 1f). Thus, CTD
109 may facilitate the folding of CSD to restore full binding to miR223.

110 YBX1-F85A in the CSD domain was reported to block the YBX1-specific
111 binding of mRNA (Lyons et al., 2016). Purified YBX1-F85A protein failed to
112 bind miR223 (Figure 1g, Figure 1 supplement 1c). These data suggest that
113 YBX1 directly and specifically binds miR223 via the CSD. The CTD of
114 YBX1 did not appear to directly bind miR223 but may facilitate a higher
115 affinity interaction with miR223.

116

117 **Finding the miR223 binding motif for binding with YBX1 and**
118 **enrichment into exosomes**

119 We next sought to determine the miR223 sequence motif responsible for
120 interaction with YBX1 and enrichment into exosomes. We used an EMSA
121 competition assay with a series of miR223 mutants. Purified YBX1 and 5'

122 fluorescently labeled miR223 were incubated with miR223 mutant
123 constructs titrated in a range from 1nM to 1μM. miR223 variants in a
124 binding domain should not compete for interaction of YBX1 with 5'
125 fluorescently tagged miR223 whereas variations in sequences irrelevant to
126 interaction would compete. Using this EMSA competition assay to screen
127 the miR223 binding motif, we found that the binding affinity of miR223mut
128 (3-6) and miR223mut (4-7) were decreased (Figure 2 supplement 1). This
129 suggested that the sequence UCAGU was critical for interaction with YBX1.
130 To test this directly, we employed a variant sequence, termed miR223mut,
131 where the UCAGU was substituted with AGACA. As a positive control, we
132 employed a variant of miR190, miR190sort, where the sequence AUAUG
133 was substituted with UCAGU (Figure 2a). EMSA data showed a reduced
134 YBX1 interaction of ~ 50-fold with miR223mut whereas the affinity of
135 miR190sort with YBX1 was increased ~10 fold compared with the
136 respective wt sequences.

137 To test whether this motif is critical for miR223 enrichment into exosomes,
138 we purified exosomes from 293T cells transiently transfected to
139 overexpress one of the four miRNA constructs (Figure 2d). RT-qPCR data
140 showed that the level of miR223 in exosomes was ~ 4-fold dependent on
141 the putative exosomal sorting motif (Figure 3e) and the enrichment of
142 miR190sort into exosomes was increased ~5-fold compared to miR190 WT
143 (Figure 2f).

144 In previous work, we developed a cell-free reaction to test the biochemical
145 requirement for YBX1 in the sorting of miR223 into vesicles formed with
146 membranes and cytosol isolated from broken HEK293 cells (Shurtleff et al.
147 2016). We have now refined this assay to measure the incorporation of ^{32}P-

148 5’ end-labeled wt and mutant miR223 into vesicles formed *in vitro*. After
149 incubation of permeabilized cells and isolated cytosol with ^{32}P-labled wt or
150 mutant miR223 at 30 °C for 20min, RNase I was added to digest any
151 unpackaged miRNA and in controls with 1% Triton X-100 to measure
152 background RNase resistant radiolabel. Samples were resolved on a gel
153 for visual and quantitative evaluation of membrane sequestered RNA
154 (Figure 2g and 2h). This data suggested that the UCAGU motif is critical for
155 miR223 packaging into vesicles in the cell-free reaction.

156 Taken together the results in Fig. 2 show that the miR223 sequence
157 UCAGA is a sorting signal for binding YBX1, for sorting this miRNA into
158 vesicles as a prelude to secretion and for the export of miR223 in
159 exosomes secreted from HEK293 cells.

160

161 **Mitochondria contribute to miR223 enrichment into exosomes.**

162 In a recent study we showed that YBX1 is sorted into P-bodies in cells and
163 that these biomolecular condensates may initiate the sorting of miR223 into
164 vesicles budding into the interior of endosomes (Liu *et al.*, 2021; Shurtleff *et*
165 *al.*, 2016). Mitochondria represent another apparent intracellular location of
166 miR223 (Wang et al., 2020). We sought to evaluate the localization of
167 miR223 in cells using transfected fluorescently tagged RNA. Hela cells
168 expressing Tom22-mCherry as a mitochondrial marker were transiently
169 transfected with fluorescently labeled miR223 and evaluated by confocal
170 fluorescence microscopy and fluorescence intensity analysis. The
171 exogenous miR223 appeared coincident with the mitochondrial marker
172 protein (Figure 3a).

173 We then used cell fractionation of homogenates of HEK293 cells to
174 evaluate the subcellular distribution of endogenous miR223. Fractionation
175 was evaluated by immunoblot using marker proteins characteristic of
176 various cell organelles (Figure 3b). RNA extracted from isolated
177 membranes confirmed that miR223 but not miR190 was significantly
178 enriched in mitochondria but not in ER or cytosol (Figure 3c, Figure 3
179 supplement 1a) (Wang *et al.*, 2020).

180 To determine the organization of miR223 on or within mitochondria, we
181 prepared mitoplasts using digitonin to strip away the mitochondrial outer
182 membrane followed by fractionation on a Percoll density gradient.
183 Immunoblots of the enriched mitochondria and isolated mitoplasts showed
184 that the outer membrane, marked by Tom20, was largely removed with
185 retention of the inner membrane marker Tim23 (Figure 3d). RNA was
186 extracted from the purified mitoplast and RT-qPCR data indicated that
187 miR223 was enriched along with mRNA for COX1, but not with nuclear U6
188 snRNA (Figure 3e). We also used IP to purify mitochondria (Figure 3
189 supplement 1b) and either Triton X-100 to solubilize the membrane or
190 freeze-thaw to allow the matrix and envelope fractions to be separated by
191 centrifugation. Mitochondrial membrane proteins, such as Tom20 and COX
192 IV, were solubilized and retained in the supernatant fraction (Figure 3
193 supplement 1c). The freeze-thaw regimen released citrate synthase to a
194 supernatant fraction whereas Tom20 and COXIV sedimented in the pellet
195 fraction. RNA was extracted from the detergent supernatant and pellet
196 fractions where we found by RT-qPCR similar distributions of COX1 and
197 miR223 suggesting that COX1 mRNA and miR223 were not as readily
198 solubilized as the inner and outer membrane proteins (Figure 3 supplement

199 1d). RT-qPCR quantification of fractions from the freeze-thaw regimen
200 showed that both COX1 mRNA and miR223 remained largely associated
201 with the sedimentable membrane fraction (Figure 3 supplement 1e). We
202 conclude that miR223 is enclosed within mitochondria, possibly in
203 association with the inner membrane.

204 We sought a further test of the cellular location of miR223 within cells. For
205 this purpose, we generated cells depleted of mitochondria (Correia-Melo et
206 al., 2017). GFP-Parkin expressing U-2 OS cells were treated with CCCP for
207 48h, conditions that cause mitochondria to be removed by mitophagy. We
208 confirmed mitochondrial depletion after CCCP treatment by RT-qPCR of
209 mitochondrial COX1 mRNA (Figure 3f) and immunoblot of the
210 mitochondrial inner membrane marker Tim23 (Figure 3g). We then
211 compared the levels of both miR223 and miR190 from GFP-Parkin
212 expressing U-2 OS cells with and without CCCP treatment. RT-qPCR data
213 showed that miR223, but not miR190, increased 3-fold in cells treated with
214 CCCP (Figure 3h). To test the possibility that miR223 accumulated in cells
215 as a result of a failure of mobilization into exosomes, we compared the
216 miR223 levels in exosomes purified from untreated and CCCP treated cells
217 (Fig. 3i and j). We found that CCCP treatment lowered the amount of
218 miR223 in EVs 3-fold (Figure 3j). The 3-fold increase in cellular at the
219 expense of exosomal miR223 may reflect a critical role for mitochondria in
220 the mobilization of this RNA to exosomes.

221

222 **YBAP1 binds miR223 in the mitochondria and in vitro.**

223 In the course of purifying a tagged version of YBX1 from 293T cells, we
224 observed another protein that copurified and found that it corresponded to
225 YBAP1 (Figure 4a, b). Such a complex of YBX1 and YBAP1 has previously
226 been reported (Matsumoto et al., 2005). We confirmed that purified YBX1
227 and YBAP1 bind each other by coexpression and affinity purification from
228 insect cells (Figure 4 supplement 1b). YBAP1 is a mitochondrial matrix
229 protein with a standard N-terminal transit peptide sequence (Muta et al.,
230 1997). We confirmed this mitochondrial localization in U-2 OS cells
231 expressing Tom22-mCherry transiently transfected with a YBAP1-GFP
232 construct (Figure 4c-d). We also showed that YBAP1 is localized within
233 mitochondria by performing a proteinase K protection assay on purified
234 mitochondria. Mitochondria were isolated from non-transfected cells and
235 exposed to proteinase K in the presence or absence of Triton X-100 and
236 the degradation of YBAP1 was evaluated by immunoblot. YBAP1 was
237 resistant to proteinase K digestion as was the mitochondrial inner
238 membrane marker Tim23 and degraded upon membrane permeabilization
239 with Triton X-100 (Figure 4e), consistent with the localization of YBAP1
240 within mitochondria.

241 To test whether YBAP1 was bound to miR223 in mitochondria, we used
242 YBAP1 immunoprecipitation with mitochondria purified by fractionation on a
243 Percoll density gradient (Figure 4f). RT qPCR data showed that
244 mitochondrial miR223 was immunoprecipitated by YBAP1 antibody but not
245 by a control antibody (Figure 4g). To determine whether the YBAP1 and
246 miR223 interaction was direct, we used the EMSA assay and found that
247 purified YBAP1 bound miR223, but not miR190. The YBAP1 interaction
248 with miR223 was not dependent on the RNA sequence motif to which

249 YBX1 bound (Figure 4 supplement 2a-b). Taken together, these data
250 suggest that YBAP1 binds miR223 in the mitochondria and in vitro.

251 **YBAP1 may control the transit of miR223 from mitochondria to**
252 **exosomes**

253 To investigate the function of YBAP1 in the transit of miR223 into
254 exosomes, we generated a 293T YBAP1 KO cell line and compared the
255 level of miR223 enrichment in exosomes and mitochondria isolated from
256 WT and mutant cells (Figure 5a, b). RT-qPCR analysis showed that
257 miR223 decreased 2-fold in mitochondria but increased 2-fold in exosomes
258 purified from mutant and WT cells (Figure 5c, d). This apparent inverse
259 relationship is consistent with a role for YBAP1 protein in the retention of
260 miR223 in mitochondria.

261

262 **YBX1 puncta shuttled from mitochondria to endosomes**

263 In previous work we reported the localization of YBX1 to P-bodies and
264 suggested this may represent an intermediate stage in the concentrative
265 sorting of miRNAs for secretion in exosomes (Liu *et al.*, 2021). In other
266 earlier work, P-bodies were seen in association with mitochondria (Huang
267 et al., 2011). To explore this possibility, we visualized endogenous YBX1
268 and YBAP1 by IF and observed YBX1 puncta colocalized with the
269 mitochondria (Figure 6a). In order to detect the proximity of endosomes to
270 this point of contact between YBX1 puncta and mitochondria, we used U-2
271 OS cells transfected with Rab5(Q79L)-mCherry, which we employed
272 previously to enlarge and detect the internalization of YBX1 into
273 endosomes (Liu *et al.*, 2021). We then used three color visualization of the

U-2 OS cells also transfected with YFP-YBX1 and mito-BFP. Time-lapse imaging showed YBX1 puncta in close proximity to mitochondria or endosomes, followed quickly by transfer between them (Figure 6b). Taken together, these data suggest a mechanism whereby miR223 stored in mitochondria, possibly sequestered by YBAP1, may be captured in a tighter interaction with YBX1 in P-bodies and delivered to endosomes for sorting and secretion in exosomes.

Discussion

Selected miRNAs are sorted, some with very high fidelity, into invaginations in the endosome that give rise to exosomes secreted from cultured human cells and likely from many if not all cells in metazoan organisms. The means by which these miRNAs are sorted and the possible extracellular functions they serve is a subject of interest in normal and disease physiology. Here we report the role of the RNA-binding protein YBX1 and a sorting signal on one target RNA, miR223, and the indirect path miR223 may take from storage in mitochondria into exosomes.

We have identified a sorting signal on miR223, UCAGU, responsible for high affinity interaction with YBX and for sorting into vesicles formed in a cell-free reaction as well as for secretion in exosomes by HEK293 cells. The YBX1 protein has three distinct domains, one of which, the cold-shock domain (CSD) appears to be the principal site for RNA binding, including at least one critical residue, F85, required for binding miR223 as well as other RNAs (Lyons *et al.*, 2016). The C-terminal domain (CTD) includes an intrinsically disordered domain (IDR) that promotes the formation of a

liquid-liquid phase separation likely responsible for the organization of YBX1 in P-bodies(Liu *et al.*, 2021). This domain does not itself interact with RNA, but it appears to facilitate the folding or stabilization of the CSD to promote high affinity binding to miR223.

In other work using a similar approach, we identified two separate sorting signals, a 5'UGGA and a 3'UUU, on miR122 to which the RNA-binding protein La binds *en route* to secretion in exosomes by the breast cancer cell line MDA-MB-231(Temoche-Diaz *et al.*, 2019). Other distinct sorting signals and their cognate RNA-binding proteins have been documented in different cell lines. miRNAs with a GGAG sorting motif recognized by a sumolyated form of hnRNPA2B1 was shown to be enriched in exosomes (Villarroya-Beltri *et al.*, 2013). Another sequence, AAUGC, was found to be enriched in exosomal miRNA and dependent on the RNA-binding protein FMR1 for miRNA secretion (Wozniak et al., 2020). Diverse cell lines and likely tissues appear to invoke distinct sorting signals decoded by different RNA-binding proteins. Many of the proteins may engage in biomolecular condensates such as P-bodies as a mechanism to sort RNAs for secretion (Liu *et al.*, 2021).

miR223 appears to be an example of a number of small nuclear-encoded RNAs localized to mitochondria (Jeandard et al., 2019). In some cases these RNAs, such as tRNAs, serve an essential function such as in mitochondrial protein synthesis, however, for miRNAs with no obvious mitochondrial genome target, the function remains unclear (Jeandard *et al.*, 2019). Nonetheless, others have documented the localization of these miRNAs enclosed within the mitochondrion and in the case of miR223, it appears to be tightly associated with the inner membrane. The exact

organization and function of miR223 in this location remains to be investigated but in the context of exosomal secretion, the mitochondrial localization appears to serve as a reservoir.

In relation to the mitochondrial localization of miR223, we found a mitochondrial RNA-binding protein, YBAP1, that copurified with a tagged form of YBX1 expressed in HEK293 cells. YBAP1 has previously been reported to interact with YBX1 and independently found associated with mitochondria where its localization is dependent on an N-terminal transit peptide sequence (Muta *et al.*, 1997). The association of mitochondrial YBAP1 and cytoplasmic YBX1 was reproduced by coexpression of recombinant forms of the two proteins in Baculovirus-infected SF9 cells (Figure 4 supplement 1b). YBAP1 binds miR223 selectively but with an affinity significantly below that of YBX1 (Figure 4h-j). Although YBX1 does not localize to the mitochondrion, the stable interaction of the complex may suggest a transient relationship, perhaps during the biogenesis of YBAP1 as it transits from the cytoplasm into the mitochondrion.

A functional relationship between YBAP1 and YBX1 is suggested by the reduction in miR223 in mitochondria and increase in secretion of miR223 in exosomes secreted from YBAP1 KO cells (Fig. 5). In contrast, removal of mitochondria by treatment of cells with CCCP resulted in an increase in cytoplasmic miR223 at the expense of secretion in exosomes (Fig. 3). Although YBAP1 may facilitate the retention of miR223 within mitochondria, mitochondrial RNA import and export may serve an independent role in the selective capture of miRNAs by YBX1 in cytoplasmic P-body condensates. YBX1 puncta appear to shuttle between mitochondria and endosomes at

350 which point miR223 bound to YBX1 may be further sorted into
351 invaginations budding into the interior of endosomes.

352 The highly selective nature of miRNA sorting and secretion in exosomes
353 suggests an important role in the trafficking of miRNAs between cells.
354 Numerous studies have suggested a role for secreted miRNAs in recipient
355 cells (Cha et al., 2015; Mittelbrunn et al., 2011; Pegtel et al., 2010; Valadi
356 et al., 2007). Nonetheless, as miRNAs ordinarily act stoichiometrically on
357 target mRNAs, the extremely low abundance and copy number of
358 miRNAs/vesicle is hard to reconcile with such a functional role of secreted
359 miRNA (Chevillet et al., 2014; Shurtleff et al., 2017) . Our observation that
360 the bulk of cellular miR223 is held within mitochondria suggests an
361 alternative role in some structural or regulatory process, perhaps essential
362 for mitochondrial homeostasis, controlled by the selective extraction of
363 unwanted miRNA into RNA granules and further by secretion in exosomes.

364

365

366

367

368

369

370

371

372

373 # Materials and methods

374 ## Key resources table

Reagent type (species) or resource	Designation	Source or reference	Identifiers	Additional information
Cell line (Spodoptera frugiperda)	Sf9	Other		Cell culture facility at UC Berkeley
Cell line (Homo sapiens)	HEK 293T cells	Other		Cell culture facility at UC Berkeley
Cell line (Homo sapiens)	HEK 293T-YBX1 KO cells	Other		Obtained by CRISPR-Cas9 in Schekman Lab
Cell line (Homo sapiens)	HEK 293T-YBAP1 KO	This study		Obtained by CRISPR-Cas9 in Schekman Lab
Cell line (Homo sapiens)	HEK 293T-3xHA-EGFP-OMP25	This study		Obtained by overexpression of pLJM1-3XHA-EGFP-OMP25 in Schekman lab
Cell line (Homo sapiens)	U-2OS cells			
Cell line (Homo sapiens)	U-2OS Parkin-GFP cells	This study		Obtained by overexpression of Parkin-GFP in Schekman lab
Recombinant DNA reagent	pFastBac His6 MBP N10 TEV LIC cloning vector (4C)	Addgene	RRID: Addgene_30116	N/A
Recombinant DNA reagent	Tom22-mCherry (plasmid)	This study		Gift of Dr Li Yu lab
Recombinant DNA reagent	His-MBP-YBX1 (plasmid)	This study		To express YBX1 in insect cells. Plasmid

				maintained in Schekman lab
Recombinant DNA reagent	His-MBP-YBX1(1-51) (plasmid)	This study		To express YBX1(1-51) in insect cells. Plasmid maintained in Schekman lab
Recombinant DNA reagent	His-MBP-YBX1(52-129) (plasmid)	This study		To express YBX1(52-129) in insect cells. Plasmid maintained in Schekman lab
Recombinant DNA reagent	His-MBP-YBX1(130-324) (plasmid)	This study		To express YBX1(1-51) in insect cells. Plasmid maintained in Schekman lab
Recombinant DNA reagent	His-MBP-YBX1(1-129) (plasmid)	This study		To express YBX1(1-129) in insect cells. Plasmid maintained in Schekman lab
Recombinant DNA reagent	His-MBP-YBX1(F85A) (plasmid)	This study		To express YBX1(F85A) in insect cells. Plasmid maintained in Schekman lab
Recombinant DNA reagent	His-MBP-YBAP1 (plasmid)	This study		To express YBAP1 in insect cells. Plasmid maintained in Schekman lab
Recombinant DNA reagent	Mito-BFP			Gift of Dr. Samantha Lewis lab
Recombinant DNA reagent	mCherry-Rab5(Q79L) (plasmid)	Addgene	RRID: Addgene_35138	
Recombinant DNA reagent	pLJM1-3XHA-EGFP-OMP25	This study		To express 3xHA-EGFP-OMP25 in HEK293T cells. Plasmid maintained

				in Schekman lab
Antibody	Anti-YBX1 (Rabbit polyclonal)	Abcam	RRID: AB_1950384	WB 1:1000
Antibody	Anti-YBAP1 (Mouse monoclonal)	Santa Cruz	RRID: AB_10611471	WB 1:1000
Antibody	Anti-YBAP1(Rabbit polyclonal)	Thermo Fisher Scientific	RRID: AB_2638956	WB 1:1000
Antibody	Anti-Tim23 (Mouse monoclonal)	BD Biosciences	RRID: AB_398754	WB 1:1000
Antibody	Anti-Tom20 (Mouse monoclonal)	Abcam	RRID: AB_945896	WB 1:1000
Antibody	Anti-Calnexin (Rabbit polyclonal)	Abcam	RRID: AB_2069006	WB 1:2000
Antibody	Anti-HA (Rabbit monoclonal)	Cell Signaling	RRID: AB_1549585	WB 1:1000
Antibody	Anti-COX IV (Rabbit Monoclonal)	Cell signaling	RRID: AB_2085424	WB 1:1000
Antibody	Anti-Citrate Synthase (Rabbit monoclonal)	Cell signaling	RRID: AB_2665545	WB 1:1000
Antibody	Anti-Rab5 (Rabbit monoclonal)	Cell signaling	RRID: AB_2300649	WB 1:1000
Antibody	Anti-LAMP1 (Rabbit monoclonal)	Cell signaling	RRID: AB_2687579	WB 1:1000
Antibody	Anti-GRP78 (Rabbit polyclonal)	Abcam	RRID: AB_2119834	WB 1:3000
Antibody	Anti-GADPH (Rabbit monoclonal)	Cell signaling	RRID: AB_561053	WB 1:5000
Antibody	Anti-alpha Tubulin (Mouse monoclonal)	Abcam	RRID: AB_2241126	WB 1:5000

Antibody	Anti-beta Actin (Mouse monoclonal)	Abcam	RRID: AB_449644	WB 1:5000
Software, algorithm	Image Studio Lite	LICOR		https://www.licor.com/bio/image-studio-lite/
Software, algorithm	FIJI	NIH	RRID: SCR_002285	https://fiji.sc/
Software, algorithm	GraphPad Prism	Other	RRID: SCR_002798	https://www.graphpad.com

375

376 **Cell lines and cell culture**

377 HEK 293T cells were cultured in DMEM with 10% FBS(VWR), NEAA
378 (Gibco, Cat No: 11140050) and 1mM Sodium Pyruvate (Gibco, Cat No:
379 11360070). For exosome production, we seeded cells at 10~20%
380 confluency in 150 mm tissue culture dishes (Fisher Scientific, Cat No: 12-
381 565-100) containing 30ml of exosome-free medium. Exosomes were
382 collected from 80% confluent cells (~48h).

383 **Extracellular vesicle purification**

384 Conditioned medium was harvested from 80-90% confluent HEK 293T
385 cultured cells. All procedures were performed at 4 ℃. Cells and large debris
386 were removed by centrifugation in a Sorvall R6+ centrifuge at 1,000xg for
387 15 min followed by 10,000xg for 15 min using a FIBERlite F14-6x500y rotor.
388 The supernatant fraction was then centrifuged onto a 60% sucrose cushion
389 which contained 10mM HEPES (pH 7.4) and 0.85% w/v NaCl at ~100,000
390 x g (28,000 RPM) for 1.5h in a SW32Ti rotor. The interface over the
391 sucrose cushion was collected and pooled for an additional centrifugation
392 onto a 2ml 60% sucrose cushion at ~120,000 x g (31,500 RPM) for 15h

using an SW41Ti rotor. The first collected interface was measured by refractometry and adjusted a sucrose concentration not exceeding 21%. For bulk purification, the EVs collected from the interface over the sucrose cushion after the first SW41Ti centrifugation were mixed with 60% sucrose to a final volume of 10ml (the concentration of sucrose ~50%). One ml of 40% and 1ml of 10% sucrose were sequentially overlaid and the samples were centrifuged at ~150,000 x g (36,500 rpm) for 15h in an SW41Ti rotor. The EVs were located at the 10%/40% interface and collected for RNA extraction or immunoblot.

Isolation of Mitochondria and Mitoplast

Mitochondria were isolated according to a well-established published protocol (Wang *et al.*, 2020). HEK293T Cells were harvested at 80% confluency and were homogenized in 6 vol of HB buffer (225 mM mannitol, 25 mM sucrose, 0.5% BSA, 0.5 mM EGTA, 30 mM Tris–HCl, pH 7.4, and protease inhibitors) in a prechilled Dounce homogenizer (Kontes), centrifuged and the postnuclear supernatant was collected. Crude mitochondria were centrifuged at 6,300 x g for 8 min, washed once with MRB buffer (250 mM mannitol, 0.5 mM EGTA, and 5 mM HEPES, pH 7.4), resuspended in 1ml MRB buffer, laid over a 30% Percoll solution (9ml) and centrifuged at 95,000g for 45min. The buoyant, purified fraction of mitochondria was collected for further analysis. For mitoplast purification, crude mitochondria were resuspended into 10 vol MRB buffer with 0.2 mg/ml digitonin and incubated on ice for 15 min~~s~~. Digitonin-treated crude mitochondria were laid over a 30% Percoll solution (9ml) and centrifuged at 95,000g for 45 min. A buoyant, purified fraction of mitoplasts was collected for further analysis.

419 **YBAP1 Immunoprecipitation from mitochondria**

420 After the Percoll gradient purification, the enriched mitochondria were
421 diluted 2x into MRB buffer and centrifuged at 12,000g for 10 min. The
422 mitochondrial pellet was lysed in 0.5ml RIPA buffer (50mM Tris-HCl, pH 7.5,
423 150mM NaCl, 2mM EDTA, 1% DDM, 1mM PMSF) containing protease
424 inhibitors (1mM 4-aminobenzamidine dihydrochloride, 1 µg/ml antipain
425 dihydrochloride, 1 µg/ml aprotinin, 1 µg/ml leupeptin, 1 µg/ml chymostatin,
426 1 mM phenylmethylsulphonyl fluoride, 50 µM N-tosyl-L-phenylalanine
427 chloromethyl ketone and 1 µg/ml pepstatin) and RNase inhibitors. The
428 mitochondrial lysate was centrifuged at 12,000g for 10 min. The
429 supernatant fraction was incubated with 10ul washed protein A Dynabeads
430 (ThermoFisher Scientific, Catalog number: 10001D) and 0.5ug mouse
431 monoclonal IgG antibody and rotated at 4 ℃ for 1h. The supernatant was
432 collected after a magnetic rack was used to remove protein A beads and
433 incubated with 40ul washed protein A Dynabeads and 4ug YBAP1 antibody
434 or mouse IgG antibody and rotated at 4 ℃ overnight. The beads were
435 collected using a magnetic rack, washed 3x with 1ml of RIPA buffer, and
436 collected for immunoblot and RNA extraction.

437 **Mitochondria-Immunoprecipitation**

438 Mito-IP was performed as previously described with slight modifications
439 (Chen et al., 2016). The mito-IP cell-line was grown to ~90% confluency in
440 15cm dishes. All the subsequent steps of mito-IP were performed using
441 ice-cold buffers either in a cold-room or on ice. The cells ($2x10^7$) were
442 washed twice with 10ml of PBS. Cells were then harvested in 10ml of mito-

443 IP buffer (10mM KH2PO4, 137mM KCl) containing protease inhibitors
444 (1mM 4-aminobenzamidine dihydrochloride, 1 µg/ml antipain
445 dihydrochloride, 1 µg/ml aprotinin, 1 µg/ml leupeptin, 1 µg/ml chymostatin,
446 1 mM phenylmethylsulphonyl fluoride, 50 µM N-tosyl-L-phenylalanine
447 chloromethyl ketone and 1 µg/ml pepstatin) and TCEP 0.5mM. The final
448 mito IP buffer also contained 6ml of OptiPrep™ (Sigma®) per 100ml. Cells
449 were collected at 700xg for 5 min and resuspended in 1ml of mito-IP buffer
450 per 15cm plate. Cells were then lysed using 5-10 passes through a 22G
451 needle and a post-nuclear supernatant (PNS) fraction was obtained after
452 centrifuging the lysate at 1500xg for 10 min to remove unbroken cells and
453 nuclei. Whenever necessary, a fraction of PNS was saved for immunoblot
454 analysis. The resulting PNS was incubated with 100 µl of anti-HA magnetic
455 beads (Sigma®) pre-equilibrated in the mito-IP buffer in 1.5ml
456 microcentrifuge tubes and then gently rotated on a mixer for 15min. The
457 beads were collected using a magnetic rack and washed 3x for 5min with
458 1ml of mito-IP buffer. To assess their quality, we assayed the
459 immunoprecipitated mitochondria for the following protein markers by
460 immunoblotting using the rabbit primary antibodies- anti-HA (1:1000), anti-
461 COX IV (1:1000), anti-TOM20 (1:1000), anti-Citrate Synthase (1:1000),
462 anti-RAB5 (1:1000), anti-LAMP1 (1:2000), anti-GAPDH (1:5000), and anti-
463 GRP78 (Abcam®) (1:3000). All of the above antibodies were sourced from
464 Cell Signaling Technology®, unless stated otherwise. As a negative control,
465 non-transduced HEK293T cells were used in these experiments to assess
466 the non-specific capture of the marker proteins.

467 **Mitochondrial Fractionation**

468 One mito-IP was performed per sample as described above. To ensure an
469 even distribution of mitochondria across the samples, we pooled washed
470 beads from all the IPs and equally distributed aliquots for subsequent
471 treatments. Mitochondria were lysed in a 50µl final volume using either 1%
472 vol/vol Triton X-100 (final concentration) or by three sequential rounds of
473 freeze/thaw using liquid-nitrogen, as indicated. Urea was added to a final
474 concentration of 3M. After a 10 min incubation on ice, samples were
475 centrifuged at 15000xg for 15 min and supernatant and pellet fractions
476 were collected as indicated. The total fractionated mitochondria were
477 analyzed by immunoblotting for various mitochondrial markers. To analyze
478 the specific RNA content of total or fractionated mitochondria, we extracted
479 RNA using Trizol™ (Invitrogen®) as per manufacturer's recommendations
480 followed by q-PCR.

481 **In vitro packaging of miR223 and miR223mut**

482 Preparation of membranes and cytosol

483 The membrane and cytosol fractions were prepared from HEK293T cells as
484 previously described with slight modifications (Shurtleff *et al.*, 2016;
485 Temoche-Diaz *et al.*, 2020). All steps were carried out in either the cold-
486 room or on ice using ice-cold buffers and pre-chilled equipment. Briefly,
487 HEK293T cells (80% confluency) were washed twice with PBS and then
488 harvested in the homogenization buffer (HB) (250 mM sorbitol, 20mM
489 HEPES-KOH pH 7.4) containing protease inhibitor cocktail (1mM 4-
490 aminobenzamidine dihydrochloride, 1 µg/ml antipain dihydrochloride, 1
491 µg/ml aprotinin, 1 µg/ml leupeptin, 1 µg/ml chymostatin, 1 mM
492 phenylmethylsulphonyl fluoride, 50 µM N-tosyl-L-phenylalanine
493 chloromethyl ketone and 1 µg/ml pepstatin). The cell pellet was obtained by
494 centrifuging the cells at 500xg for 5 min. After discarding the supernatant,
495 cells were weighed and resuspended in two volumes of HB followed by
496 lysis with 5-10 passages through a 22G needle. The lysate was centrifuged
497 at 1500xg for 10 min to remove unbroken cells and nuclei to obtain a PNS.
498 The resulting PNS was centrifuged at 20,000xg for 30 min to obtain a
499 membrane fraction. The supernatant from above was centrifuged at
500 150,000xg for 30 min using a TLA-55 rotor (Beckman Coulter ®) and the
501 resulting supernatant was used as the cytosol fraction (~6mg protein/ml).
502 The membrane fraction from the first 20,000xg sedimentation was

503 resuspended in 1 ml of HB and centrifuged again at 20,000xg for 30 min.
504 The pellet fraction was resuspended in one volume of HB and rested on an
505 ice block for a minimum of 10 min until the insoluble components and
506 debris settled at the bottom of the tube. The finely resuspended material
507 was then transferred to a new microcentrifuge tube (to avoid the settled
508 debris) and was used as the membrane fraction.

509 Preparation of radiolabeled miR223 and miR223mut substrates

510 HPLC purified miR223 and miR223mut oligos were obtained from IDT®. A
511 stock solution of these oligos (1µl of a 10µM) was 5'-end-labeled using
512 T4PNK (NEB®) and 5µl of ATP, [γ-32P]- 6000Ci/mmol 10mCi/ml EasyTide
513 (PerkinElmer® BLU502Z250UC) as per manufacturer's recommendations
514 in a 50µl reaction volume. T4PNK was heat-inactivated at 70°C for 15 min.
515 Unincorporated radionucleotides were removed by passing through
516 PerformaTM spin columns (EdgeBio®). The flow-through (radiolabeled
517 substrate) was collected and stored at -20°C until further use.

518 *In vitro* miR223 packaging reaction

519 Wherever indicated, 10µl of cytosol (~5 mg/ml), 17µl of membranes, 2µl of
520 radiolabeled substrate, 9µl of 5x incorporation buffer (400 mM KCl, 100 mM
521 $CaCl_2$, 60 mM HEPES-NaOH, pH 7.4, 6 mM, MgOAc), 4.5µl of 10x ATP
522 regeneration system (400 mM creatine phosphate, 2 mg/ml creatine
523 phosphokinase, 10 mM ATP, 20 mM HEPES pH 7.2, 250 mM sorbitol, 150
524 mM KOAc, 5 mM MgOAc), 1µl of ATP (100mM, Promega®), 0.5µl of GTP
525 (100mM, Promega®), 1µl of Ribolock™ (40U/µL, Invitrogen®) were mixed to
526 setup a 45µl *in vitro* packaging reaction. In samples without the cytosol or
527 membranes, the final reaction volumes were adjusted to 45µl using HB.
528 The reactions were incubated at either 30°C or on ice, as indicated, for 15
529 min. Following the incubation, the indicated samples were subjected to
530 RNAse ONE™ (Promega®) using 10U of the enzyme in the presence of
531 urea (300mM final concentration) in a total reaction volume of 60µl.
532 Wherever indicated, TritonX-100 was added to a final concentration of 1%.
533 The RNAse treatments were carried out for 20 min at 30°C followed by
534 RNA extraction using DirectZol™ (Zymo Research®) kits as per
535 manufacturer's protocol. The RNA was precipitated overnight at -20°C by
536 the addition of 3 vol of ethanol, 1/10th volume of 3M sodium acetate (pH5.2)

537 and 30μg Glycoblue™ reagent (Invitrogen®). Precipitated RNA was
538 sedimented at 16,000xg for 30 min followed by washing with ice-cold 70%
539 ethanol. The RNA pellet was resuspended in 2X RNA loading dye (NEB®)
540 and heated for 5 min at 70°C. The RNA was separated using a 15%
541 denaturing polyacrylamide gel, followed by gel drying using a vacuum gel
542 dryer (Model 583, Biorad®). The bands were visualized by
543 phosphorimaging using a Kodak® storage phosphor screen and the Pharos
544 FX™ Plus Molecular Imager (Biorad®).

545

546 **Immunoblots**

547 Cell lysates and other samples were prepared by adding 2% SDS and
548 heated at 95 ℃ for 10mins. Protein was quantified using a BCA Protein
549 Assay Kit (Thermo Fisher Scientific) and appropriate amounts of samples
550 were mixed with 5x SDS loading buffer. Samples were heated at 95℃ for
551 10min and separated on 4–20% acrylamide Tris-glycine gradient gels (Life
552 Technologies). Proteins were transferred to PVDF membranes (EMD
553 Millipore, Darmstadt, Germany), the membrane was blocked with 5% fat-
554 free milk powder in TBST and incubated for 1 h at room temperature or
555 overnight at 4°C with primary antibodies. Blots were then washed in 3
556 washes of TBST for 10 min each. Membranes were incubated with anti-
557 rabbit or anti-mouse secondary antibodies (GE Healthcare Life Sciences,
558 Pittsburgh, PA) for 1h at room temperature and rinsed in 3 washes of TBST
559 for 10 min each. Blots were developed with ECL-2 reagent (Thermo Fisher
560 Scientific). Primary antibodies used in this study were as follows: anti-
561 Tim23 (BD, 611222), Calnexin (Abcam, ab22595), Actin (Abcam, ab8224),
562 Tubulin (Abcam, ab7291), YBAP1 (Santa Cruz Biotechnology, sc-271200).

563 **Immunofluorescence**

564 Cells were cultured on 12mm round coverslips (corning) and were fixed
565 with 4% EM-grade paraformaldehyde (Electron Microscopy Science,
566 Hatfield, PA) in PBS pH7.4 for 10 min at room temperature. Cells were then
567 washed 3x with PBS for 10min each, treated with permeabilizing buffer (10%
568 FBS in PBS) containing 0.1% saponin for 20min and treated in blocking
569 buffer for 30min. Subsequently, cells were incubated with primary
570 antibodies in permeabilizing buffer for 1h at room temperature, washed 3x
571 with PBS for 10 min each and incubated with secondary antibodies in
572 permeabilizing buffer for 1h at room temperature and finally washed 3x with
573 PBS for 10 min each. Cells were mounted in slides with Prolong Gold with
574 DAPI (Thermo Fisher Scientific, P36931). Primary antibody used in the
575 immunofluorescence studies were as follows: anti-YBX1 (Abcam, ab12148),
576 YBAP1 (Santa Cruz Biotechnology, sc-271200). Images were acquired with
577 Zeiss LSM900 confocal microscope and analyzed with the Fiji software
578 (http://fiji.sc/Fiji).

579 **Quantitative real-time PCR**

580 Cellular and EV RNAs were extracted using a mirVana miRNA isolation kit
581 (Thermo Fisher Scientific, AM1560) or Direct-zol RNA Miniprep kits (Zymo
582 Research). Taqman miRNA assays for miRNA detection were purchased
583 from Life Technologies. Assay numbers were: has-miR-223-3p, 002295;
584 has-mir-190–5 p, 000489; U6 snRNA, 001973. Total RNAs were quantified
585 using RNA bioanalyzer (Agilent). Taqman qPCR master mix with no
586 Amperase UNG was obtained from Life Technologies for reverse
587 transcription. For mRNA, RevertAid First Strand cDNA Synthesis Kit
588 (Thermo Scientific, K1621) was used for reverse transcription. COX1 qPCR
589 primers: Forward-5'-TCTCAGGCTACACCCTAGACCA-3', Reverse-5'-

590 ATCGGGGTAGTCCGAGTAACGT-3'. GAPDH qPCR primers: Forward-5'-
591 CTGACTTCAACAGCGACACC-3', Reverse-5'-
592 TAGCCAAATTCGTTGTCATACC-3'. Quantitative real-time PCR was
593 performed using an QuantStudio™ 5 Real-Time PCR System (Applied
594 Biosystems™)

595 **Protein Purification**

596 Twin Strep tag hybrid YBX1 was expressed and the protein was isolated
597 48h after PEI-mediated transfection of 293T cells. Cells were resuspended
598 in PBS and collected by centrifugation for 5 min at 600g. Pellet fractions
599 were resuspended in 35 ml lysis buffer (50mM Tris-HCl (PH=8),150mM
600 NaCl,1mM EDTA, 2mM DTT, 1mM PMSF and 1 x protease inhibitor
601 cocktail). After sonication of the cell suspension the crude lysate was
602 centrifuged for 60 min at 20,000 rpm at 4 °C. The resulting supernatant
603 fraction was incubated with 2 ml Strep-Tactin® Sepharose® resin (IBA, 2-
604 1201-010) for 1 h. Strep-Tactin® Sepharose® resin samples were
605 transferred to columns (18ml) and protein-bound beads were washed with
606 60ml wash buffer (50mM Tris-HCl (PH=8), 500mM NaCl, 1mM EDTA, 2mM
607 DTT) until no protein was eluted as monitored by the Bio-Rad protein assay
608 (Bio-Rad, Catalog #5000006). Proteins were eluted with 10 ml elution
609 buffer (50mM Tris-HCl (PH=8),150mM NaCl, 10mM desthiobiotin, 1mM
610 EDTA, 2mM DTT) and concentrated using an Amicon Ultra Centrifugal
611 Filter Unit (50 kDa, 4 ml) (Fisher Scientific, EMD Millipore). Proteins were
612 further purified by gel filtration chromatography (Superdex-200, GE
613 Healthcare) with columns equilibrated in storage buffer (50 mM Tris-HCl
614 7.4, 500 mM KCl, 5 % glycerol, 1 mM DTT). Peak fractions corresponding
615 to the appropriate fusion protein were pooled, concentrated, and distributed

616 in 10 µl aliquots in PCR tubes, flash-frozen in liquid nitrogen and stored at -
617 80 °C. Protein concentration was determined by known concentrations of
618 BSA assessed by Coomassie Blue staining.

619 Tagged (6xHis) and maltose-binding protein hybrid genes were expressed.
620 In baculovirus-infected SF9 insect cells (Lemaitre et al., 2019). Insect cell
621 cultures (1 l, $1x10^6$ cells/ml) were harvested 48 h after viral infection and
622 collected by centrifugation for 20 min at 2000 rpm. The pellet fractions were
623 resuspended in 35 ml lysis buffer (50 mM Tris-HCl 7.4, 0.5 M KCl, 5 %
624 glycerol, 10mM il~~l~~midazole, 0.5 µl/ml Benzonase nuclease (Sigma, 70746–
625 3), 1 mM DTT, 1 mM PMSF and 1 x protease inhibitor cocktail). Cells were
626 lysed by sonication and the crude lysate was centrifuged for 60 min at 20,
627 000 rpm at 4 °C. After centrifugation, the supernatant fraction was
628 incubated with 2 ml Ni-NTA His-Pur resin (Thermo Fisher, PI88222) for 1 h.
629 Ni-NTA resin samples were transferred to columns (18ml) and protein-
630 bound beads were washed with 60ml lysis buffer until no protein was eluted
631 as monitored by the Bio-Rad protein assay (Bio-Rad, Catalog #5000006).
632 Proteins were eluted with 10 ml elution buffer (50 mM Tris-HCl 7.4, 0.5 M
633 KCl, 5 % glycerol, 500mM imidazole). The eluted sample was incubated
634 with 2 ml amylose resin (New England Biolabs, E8021L) for 1 h at 4°C.
635 Amylose resin samples were transferred to columns and protein-bound
636 beads were washed with 60ml lysis buffer until no protein was eluted as
637 monitored by the Bio-Rad protein assay. Proteins were eluted with 10 ml
638 elution buffer (50 mM Tris-HCl 7.4, 500 mM KCl, 5 % glycerol, 50 mM
639 maltose). Proteins were concentrated using an Amicon Ultra Centrifugal
640 Filter Unit (50 kDa, 4 ml) (Fisher Scientific, EMD Millipore). Proteins were
641 further purified by gel filtration chromatography (Superdex-200, GE

642 Healthcare) with columns equilibrated in storage buffer (50 mM Tris-HCl
643 7.4, 500 mM KCl, 5 % glycerol, 1 mM DTT). Peak fractions corresponding
644 to the appropriate fusion protein were pooled, concentrated, and distributed
645 in 10 µl aliquots in PCR tubes, flash-frozen in liquid nitrogen and stored at
646 –80 °C. Protein concentration was determined by known concentrations of
647 BSA based on Coomassie Blue staining.

648 **CRISPR/Cas9 genome editing**

649 A pX330-based plasmid expressing Venus fluorescent protein (Shurtleff *et*
650 *al.*, 2016) was used to clone the gRNAs targeting YBAP1. A CRISPR guide
651 RNA targeting the first exon of the YBAP1 open reading frame was
652 designed following the CRISPR design website
653 (http://crispor.tefor.net/crispor.py): CGCTGCGTGCCCCGTGTGCT.
654 Oligonucleotides encoding gRNAs were annealed and cloned into pX330-
655 Venus as described (Cong et al., 2013). HEK293T cells were transfected
656 by Lipofectamine 2000 for 48h at low passage number, trypsinized and
657 sorted for single, Venus positive cells in 96 well plates by a BD Influx cell
658 sorter. YBAP1 knockout candidates were confirmed by immunoblot. HEK
659 293T YBX1 knockout cells were generously provided by Dr. Xiaoman Liu
660 (Liu *et al.*, 2021).

661 **Electrophoretic mobility shift assay**

662 Fluorescently labeled RNAs (5'-IRD800CWN) were ordered from Integrated
663 DNA Technologies (IDT, Coralville, IA) for detecting free and protein-bound
664 RNA. EMSA was performed as described (Rio, et al., 2014) with some
665 modification. Briefly, 1 nM of IRD800CWN-labeled RNA was incubated with
666 increasing amounts of purified proteins, ranging from 500 pM - 1 µM.

667 Buffer E was used in this incubation (25 mM Tris pH8.0, 100 mM KCl, 1.5
668 mM MgCl2, 0.2 mM EGTA, 0.05% Nonidet P-40, 1 mM DTT, 5% glycerol,
669 50 ug/ml heparin). Reactions were incubated at 30 ℃ for 30min then chilled
670 on ice for 10 min. Samples were mixed with 6x loading buffer (60 mM KCl,
671 10 mM Tris pH 7,6, 50% glycerol, 0.03% (w/v) xylene cyanol). Mixtures
672 (5ul) were loaded onto a 6% native polyacrylamide gel at 200V for 45mins
673 in a cold room. The fluorescence signal was detected using an Odyssey
674 CLx Imaging System (LI-COR Biosciences, Lincoln, NE). The software of
675 the Odyssey CLx Imaging System was used to quantify fluorescence. To
676 calculate Kds, we fitted used Hill equations with quantified data points.

677

678 **Data availability**

679 All data generated or analyzed in this study are included in the manuscript
680 and supporting files. Source data files have been provided for Figure 1b,
681 Figure 1c, Figure 1f, Figure 1g, Figure 1-figure supplement 1a-c, Figure 2b,
682 Figure 2g, Figure 2-figure supplement 1a-f, Figure 3b, Figure 3d, Figure 3g,
683 Figure 3 supplement 1b-c, Figure 4a, Figure 4b, Figure 4e, Figure 4f,
684 Figure 4h, Figure 4i, Figure 4-figure supplement 1a-b, Figure 4-figure
685 supplement 2a, Figure 5b.

686

687 **Article and author information**

688 **Author details**

689 **Liang Ma**

690 Department of Molecular and Cell Biology, Howard Hughes Medical
691 Institute, University of California, Berkeley, Berkeley, United States

692 Contribution: Conceptualization, Investigation, Methodology, Writing -
693 original draft, Writing - review and editing

694 Competing interests: No competing interests declared

695 ORCID icon 0000-0003-3227-5917

696 **Jasleen Singh**

697 Department of Molecular and Cell Biology, Howard Hughes Medical
698 Institute, University of California, Berkeley, Berkeley, United States

699 Contribution: Contribution of mito-IP, mitochondrial fractionation, and in
700 vitro packaging assay

701 Competing interests: No competing interests declared

702 **Randy Schekman**

703 Department of Molecular and Cell Biology, Howard Hughes Medical
704 Institute, University of California, Berkeley, Berkeley, United States

705 Contribution: Conceptualization, Funding acquisition, Investigation,
706 Supervision, Writing - review and editing

707 For correspondence: schekman@berkeley.edu

708 Competing interests: Reviewing editor, eLife

709 ORCID icon 0000-0001-8615-6409

710 **Funding**

Howard Hughes Medical Institute (Investigator) and Aligning Science Across Parkinson's Disease

Randy Schekman

The funders had no role in study design, data collection and interpretation, or the decision to submit the work for publication.

Acknowledgements

We thank Dr. Samantha Lewis for advice about localization to mitochondria and for sharing a plasmid; thanks Matthew J Shurtleff, David Melville, Shenjie Wu, Jordan Ngo, Congyan Zhang, Justin Williams, Morayma M Temoche-Diaz for suggestions and reading and editing the manuscript. We also thank staff at the UC Berkeley shared facilities, the Cell Culture Facility, the Flow Cytometry Facility and QB3-Berkeley (The California Institute for Quantitative Biosciences at UC Berkeley). LM and JS are supported as Research Associates of the HHMI. RS is an Investigator of the HHMI, a Senior fellow of the UC Berkeley Miller Institute of Science and Scientific Director of Aligning Science Across Parkinson's Disease.

References

Cha, D.J., Franklin, J.L., Dou, Y., Liu, Q., Higginbotham, J.N., Demory Beckler, M., Weaver, A.M., Vickers, K., Prasad, N., Levy, S., et al. (2015). KRAS-dependent sorting of miRNA to exosomes. Elife *4*, e07197. 10.7554/eLife.07197.

Chen, W.W., Freinkman, E., Wang, T., Birsoy, K., and Sabatini, D.M. (2016). Absolute Quantification of Matrix Metabolites Reveals the Dynamics of Mitochondrial Metabolism. Cell *166*, 1324-1337 e1311. 10.1016/j.cell.2016.07.040.

Chevillet, J.R., Kang, Q., Ruf, I.K., Briggs, H.A., Vojtech, L.N., Hughes, S.M., Cheng, H.H., Arroyo, J.D., Meredith, E.K., Gallichotte, E.N., et al. (2014).

Quantitative and stoichiometric analysis of the microRNA content of exosomes. Proc Natl Acad Sci U S A *111*, 14888-14893. 10.1073/pnas.1408301111.
Cocucci, E., Racchetti, G., and Meldolesi, J. (2009). Shedding microvesicles: artefacts no more. Trends Cell Biol *19*, 43-51. 10.1016/j.tcb.2008.11.003.
Cong, L., Ran, F.A., Cox, D., Lin, S., Barretto, R., Habib, N., Hsu, P.D., Wu, X., Jiang, W., Marraffini, L.A., and Zhang, F. (2013). Multiplex genome engineering using CRISPR/Cas systems. Science *339*, 819-823. 10.1126/science.1231143.
Correia-Melo, C., Ichim, G., Tait, S.W., and Passos, J.F. (2017). Depletion of mitochondria in mammalian cells through enforced mitophagy. Nat Protoc *12*, 183-194. 10.1038/nprot.2016.159.
Harding, C., Heuser, J., and Stahl, P. (1983). Receptor-mediated endocytosis of transferrin and recycling of the transferrin receptor in rat reticulocytes. J Cell Biol *97*, 329-339. 10.1083/jcb.97.2.329.
Huang, L., Mollet, S., Souquere, S., Le Roy, F., Ernoult-Lange, M., Pierron, G., Dautry, F., and Weil, D. (2011). Mitochondria associate with P-bodies and modulate microRNA-mediated RNA interference. J Biol Chem *286*, 24219-24230. 10.1074/jbc.M111.240259.
Jeandard, D., Smirnova, A., Tarassov, I., Barrey, E., Smirnov, A., and Entelis, N. (2019). Import of Non-Coding RNAs into Human Mitochondria: A Critical Review and Emerging Approaches. Cells *8*. 10.3390/cells8030286.
Liu, X.M., Ma, L., and Schekman, R. (2021). Selective sorting of microRNAs into exosomes by phase-separated YBX1 condensates. Elife *10*. 10.7554/eLife.71982.
Lyons, S.M., Achorn, C., Kedersha, N.L., Anderson, P.J., and Ivanov, P. (2016). YB-1 regulates tiRNA-induced Stress Granule formation but not translational repression. Nucleic Acids Res *44*, 6949-6960. 10.1093/nar/gkw418.
Matsumoto, K., Tanaka, K.J., and Tsujimoto, M. (2005). An acidic protein, YBAP1, mediates the release of YB-1 from mRNA and relieves the translational repression activity of YB-1. Mol Cell Biol *25*, 1779-1792. 10.1128/MCB.25.5.1779-1792.2005.
Mittelbrunn, M., Gutierrez-Vazquez, C., Villarroya-Beltri, C., Gonzalez, S., Sanchez-Cabo, F., Gonzalez, M.A., Bernad, A., and Sanchez-Madrid, F. (2011). Unidirectional transfer of microRNA-loaded exosomes from T cells to antigen-presenting cells. Nat Commun *2*, 282. 10.1038/ncomms1285.
Mukherjee, K., Ghoshal, B., Ghosh, S., Chakrabarty, Y., Shwetha, S., Das, S., and Bhattacharyya, S.N. (2016). Reversible HuR-microRNA binding controls extracellular export of miR-122 and augments stress response. EMBO Rep *17*, 1184-1203. 10.15252/embr.201541930.
Muta, T., Kang, D., Kitajima, S., Fujiwara, T., and Hamasaki, N. (1997). p32 protein, a splicing factor 2-associated protein, is localized in mitochondrial matrix

and is functionally important in maintaining oxidative phosphorylation. J Biol Chem *272*, 24363-24370. 10.1074/jbc.272.39.24363.
Pegtel, D.M., Cosmopoulos, K., Thorley-Lawson, D.A., van Eijndhoven, M.A., Hopmans, E.S., Lindenberg, J.L., de Gruijl, T.D., Wurdinger, T., and Middeldorp, J.M. (2010). Functional delivery of viral miRNAs via exosomes. Proc Natl Acad Sci U S A *107*, 6328-6333. 10.1073/pnas.0914843107.
Santangelo, L., Giurato, G., Cicchini, C., Montaldo, C., Mancone, C., Tarallo, R., Battistelli, C., Alonzi, T., Weisz, A., and Tripodi, M. (2016). The RNA-Binding Protein SYNCRIP Is a Component of the Hepatocyte Exosomal Machinery Controlling MicroRNA Sorting. Cell Rep *17*, 799-808. 10.1016/j.celrep.2016.09.031.
Shurtleff, M.J., Temoche-Diaz, M.M., Karfilis, K.V., Ri, S., and Schekman, R. (2016). Y-box protein 1 is required to sort microRNAs into exosomes in cells and in a cell-free reaction. Elife *5*. 10.7554/eLife.19276.
Shurtleff, M.J., Yao, J., Qin, Y., Nottingham, R.M., Temoche-Diaz, M.M., Schekman, R., and Lambowitz, A.M. (2017). Broad role for YBX1 in defining the small noncoding RNA composition of exosomes. Proc Natl Acad Sci U S A *114*, E8987-E8995. 10.1073/pnas.1712108114.
Temoche-Diaz, M.M., Shurtleff, M.J., Nottingham, R.M., Yao, J., Fadadu, R.P., Lambowitz, A.M., and Schekman, R. (2019). Distinct mechanisms of microRNA sorting into cancer cell-derived extracellular vesicle subtypes. Elife *8*. 10.7554/eLife.47544.
Temoche-Diaz, M.M., Shurtleff, M.J., and Schekman, R. (2020). Buoyant Density Fractionation of Small Extracellular Vesicle Sub-populations Derived from Mammalian Cells. Bio Protoc *10*, e3706. 10.21769/BioProtoc.3706.
Teng, Y., Ren, Y., Hu, X., Mu, J., Samykutty, A., Zhuang, X., Deng, Z., Kumar, A., Zhang, L., Merchant, M.L., et al. (2017). MVP-mediated exosomal sorting of miR-193a promotes colon cancer progression. Nat Commun *8*, 14448. 10.1038/ncomms14448.
Valadi, H., Ekstrom, K., Bossios, A., Sjostrand, M., Lee, J.J., and Lotvall, J.O. (2007). Exosome-mediated transfer of mRNAs and microRNAs is a novel mechanism of genetic exchange between cells. Nat Cell Biol *9*, 654-659. 10.1038/ncb1596.
Villarroya-Beltri, C., Gutierrez-Vazquez, C., Sanchez-Cabo, F., Perez-Hernandez, D., Vazquez, J., Martin-Cofreces, N., Martinez-Herrera, D.J., Pascual-Montano, A., Mittelbrunn, M., and Sanchez-Madrid, F. (2013). Sumoylated hnRNPA2B1 controls the sorting of miRNAs into exosomes through binding to specific motifs. Nat Commun *4*, 2980. 10.1038/ncomms3980.
Wang, W.X., Prajapati, P., Nelson, P.T., and Springer, J.E. (2020). The Mitochondria-Associated ER Membranes Are Novel Subcellular Locations

816 Enriched for Inflammatory-Responsive MicroRNAs. Mol Neurobiol *57*, 2996-
817 3013. 10.1007/s12035-020-01937-y.
818 Wozniak, A.L., Adams, A., King, K.E., Dunn, W., Christenson, L.K., Hung, W.T.,
819 and Weinman, S.A. (2020). The RNA binding protein FMR1 controls selective
820 exosomal miRNA cargo loading during inflammation. J Cell Biol *219*.
821 10.1083/jcb.201912074.

822

823 **Figure legends**

824 **Figure 1.** YBX1 directly and specifically binds miR223.

825 (a.) RT-qPCR analysis of relative abundance of miR223 detected in
826 exosomes compared to cellular level at 293T WT cells or YBX1 knockout
827 cells. Data are plotted from 3 independent experiments, each independent
828 experiment with triplicate qPCR reactions; error bars represent standard
829 deviations. (b-c.) EMSA assays using 1nM 5' fluorescently labeled miR223
830 or miR190 and purified YBX1. Purified YBX1 was titrated from 500pM to
831 1μM. In gel fluorescence was detected. Quantification of (d.) shows the
832 calculated Kd. (e.) Schematic diagrams of the different domains of YBX1.
833 (f.) EMSA assay using 1nM 5' fluorescently labeled miR223 and purified
834 YBX1 truncations. [YBX1(1-51) or YBX1(52-129) or YBX1(130-324).] (g.)
835 EMSA assay using 1nM 5' fluorescently labeled miR223 and purified YBX1
836 truncations [YBX1(1-129) or YBX1(52-324)] or YBX1(F85A) mutant.

837 **Figure 1-figure supplement 1.** Purified YBX1 full length protein and
838 different truncations and mutation.

839 (a-c.) YBX1 full length protein or different truncations were overexpressed
840 and purified from insect cells.

841 **Figure 2.** miR223 sequence motif UCAGU binds YBX1

842 (a.) RNA oligonucleotides corresponding to miR223, miR190 and versions
843 with mutated sorting motif (miR223mut) or mutation to introduce the sorting
844 motif (miR190sort). (b.) EMSA assays using 1nM 5' fluorescently labeled
845 miR223 WT or miR223mut or miR190 WT or miR190sort and purified
846 YBX1. Purified YBX1 was titrated from 500pM to 1μM. In gel fluorescence
847 was detected. (c.) Binding affinity curves as calculated by EMSA data from
848 (b.) (d.) Schematic shows exosome purification with buoyant density
849 flotation in a sucrose step gradient from 293T cells overexpressing miR223
850 WT or mutant or miR190 WT or miR190sort. (e.) RT-qPCR analysis of
851 relative abundance of miR223 or miR223mut detected in exosomes
852 compared to cellular level in 293T cells overexpressing miR223 WT or
853 miR223mut. Data are plotted from 3 independent experiments and error
854 bars represent standard derivations. (f.) RT-qPCR analysis of relative
855 abundance of miR190 or miR190sort detected in exosomes compared to
856 cellular level in 293T cells overexpressing miR190 WT or miR190sort. Data
857 are plotted from 3 independent experiments and error bars represent
858 standard derivations. (g.) *In vitro* packaging assay using ^{32}P 5'end-labeled
859 miR223 and miR223mut. Cell-free packaging of miR223 and miR223mut
860 measured as protected radioactive signal from ^{32}P labeled miR223 and
861 miR223mut. Reactions with or without membrane, cytosol, and 1% Triton
862 X-100, and incubated at 4 or 30 °C are indicated. For the samples
863 containing only cytosol plus membrane at 4 °C, only one-third of the
864 samples were loaded. Each sample was supplemented with 300mM urea
865 to reduce the background signal. (h.) Data quantification showed protected
866 fraction of miR223 and miR223mut as calculated from *in vitro* packaging
867 data shown in (g.)

Figure 2-figure supplement 1. Screening of exosomal sorting motif of miR223.

EMSA competition assay to screen the exosomal sorting motif of miR223. (a.-f.) EMSA competition assay using 1nM 5' fluorescently labeled miR223, 32nM purified YBX1 protein and unlabeled miR223 or miR223mutants. Unlabeled miR223 or miR223mutants were titrated from 1nM to 1μM.

Figure 3. Mitochondria contribute to miR223 enrichment into exosomes.

(a.) Tom22-mCherry expressing HeLa cells were transfected with Atto-647 labeled miR223, cultured for 4h and observed by confocal microscopy. Scale bar, 5 μm. The data shown on the right is the fluorescence intensity of the different channels indicated by a solid white line. (b.) Immunoblot analysis of protein markers for different subcellular fractions isolated from 293T cells. (c.) RT-qPCR analysis of miR223 fold changes of different subcellular fractions isolated from 293T cells relative to cell lysate. (d.) Immunoblot analysis of protein markers for mitoplasts purified from 293T cells. (e.) RT-analysis of COX1 mRNA, miR223 and U6 snRNA fold changes for mitoplasts purified from 293T cells relative to cell lysate. (f.) RT-qPCR analysis of mitochondrial mRNA COX1 in GFP-Parkin expressing U2OS cells treated with or without CCCP. Data are plotted from 3 independent experiments and error bars represent standard derivations. (g.) Immunoblot analysis of mitochondrial marker Tim23 in GFP-Parkin expressing U2OS cells treated with or without CCCP. (h.) RT-qPCR analysis showed an increase in miR223 in GFP-Parkin expressing cells treated with CCCP. Data are plotted from 3 independent experiments and error bars represent standard derivations. (i.) Schematic of exosome purification from mitochondria-depleted GFP-Parkin expressing U2OS

894 cells. (j.) RT-qPCR analysis showing the enrichment of exosomal miR223
895 was decreased after GFP-Parkin expressing cells were treated with CCCP.
896 Data are plotted from 3 independent experiments and error bars represent
897 standard derivations.

898 **Figure 3-figure supplement 1.** miR223, but not miR190, enriched in
899 mitochondria.

900 (a.) RT-qPCR analysis of miR190 fold changes in subcellular fractions
901 isolated from 293T cells relative to cell lysate. Data are plotted from 3
902 independent experiments and error bars represent standard derivations. (b.)
903 Mitochondria immunoprecipitation. Mitochondria purified from 293T WT or
904 3xHA-EGFP-OMP25 overexpressing cell line using anti-HA magnetic
905 beads. Immunoblot detection of inner membrane marker COX IV, outer
906 membrane marker TOM20 and mitochondrial matrix protein citrate
907 synthase (CS) but not of the early endosome marker RAB5, lysosome
908 marker LAMP1, cytosol marker GAPDH and ER marker GRP78. (c.)
909 Purified mitochondria from (b.) were treated with 1% Triton X-100 or
910 freeze/thaw using liquid-nitrogen and the supernatant and pellet fractions
911 were collected after centrifugation. Immunoblot analysis of the
912 mitochondrial protein distribution of outer membrane protein TOM20, inner
913 membrane protein COX IV and matrix protein citrate synthase. (d.) and (e.)
914 RT-qPCR analysis of the distribution of COX1 mRNA and miR223 from (c.)

915 **Figure 4.** YBAP1 directly and specifically binds miR223.

916 (a.) Strep II-YBX1 was overexpressed into 293T cells. Coomassie blue
917 detection of unknown band copurified with YBX1 from 293T cells. (b.)
918 Immunoblot identifies unknown band was YBAP1. (c.) Tom22-mCherry

919 expressing U2OS was transfected with YBAP1-GFP, cultured for 12h and
920 observed by confocal microscopy. Scale bar, 10 μm. (d.) Quantification of
921 the fluorescence intensity of the different channels indicated by the solid
922 white line of (c.). (e.) YBAP1 resides in mitochondria. Proteinase K
923 protection assay for YBAP1 using purified mitochondria from 293T cells.
924 Samples were treated with or without proteinase K (10 ug/ml) and or Triton
925 X-100 (0.5%). Immunoblots for Tim23, Tom20 and YBAP1 are shown. (f.)
926 Mitochondria were purified for immunoprecipitation with YBAP1 antibody.
927 Immunoblot detection of YBAP1 and Tom20. (g.) RT-qPCR analysis of
928 miR223 fold changes of YBAP1 IP samples. Data are plotted from 3
929 independent experiments and error bars represent standard derivations. (h-
930 i.) EMSA assays using 1nM 5' fluorescently labeled miR223 or miR190.
931 Purified YBAP1 was titrated from 500pM to 1μM. In gel fluorescence was
932 detected. Quantification of (j.) shown the calculated Kd.

933 **Figure 4-figure supplement 1.** YBX1 and YBAP1 copurify as a complex
934 from transfected SF9 cells.

935 (a.) YBAP1 purified from insect cells which overexpressed His-MBP-
936 YBAP1. (b.) YBX1 and YBAP1 were copurified from insect cells which
937 overexpressed His-MBP-YBX1 and no tagged YBAP1.

938 **Figure 4-figure supplement 2.** YBAP1 does not share the same miR223-
939 binding motif as YBX1.

940 (a.) EMSA assays using 1nM 5' fluorescently labeled miR223 WT or
941 miR223mut or miR190 WT or miR190sort and purified YBAP1. Purified
942 YBAP1 was titrated from 500pM to 1μM. In gel fluorescence was detected.
943 (b.) Binding affinity curves as calculated by EMSA data from (a.)

944

945 **Figure 5.** YBAP1 sequesters miR223 which is released and secreted in
946 YBAP1 KO cells

947 (a.) Schematic shows exosome and mitochondria purification from 293T
948 WT cells and YBAP1 knock out cells for RT-qPCR analysis. (b.) Analysis of
949 293T WT and CRISPR/Cas9 genome-edited cells by immunoblot for
950 YBAP1 (top) and actin (bottom). (c.) RT-qPCR analysis of miR223
951 enrichment in mitochondria purified from 293T WT cells and YBAP1 KO
952 cells relative to cell lysate. Data are plotted from 3 independent
953 experiments and error bars represent standard derivations. (d.) RT-qPCR
954 analysis of miR223 enrichment in exosomes isolated from 293T WT cells
955 and YBAP1 KO cells relative to cell lysate. Data are plotted from 3
956 independent experiments and error bars represent standard derivations.

957 **Figure 6.** YBX1 puncta relocalize from mitochondria to endosomes.

958 (a.) YBX1 puncta on the mitochondria. U2OS cells were stained with anti-
959 YBX1 and anti-YBAP1 antibodies and observed by confocal microscopy.
960 The right panel shows enlarged regions of interest from the left panel.
961 Scale bar, 5 μm. (b.) YBX1 puncta relocalize from mitochondria to
962 endosomes. U2OS cells overexpressed YFP-YBX1, Rab5(Q79L)-mCherry
963 and mito-BFP. Time-lapse images were acquired with a Zeiss LSM900
964 confocal microscope. Scale bar, 2 μm.

965 **Figure 7.** Diagram representing a model of miR223 sorting from
966 mitochondria into exosomes.

967 Stages in the transfer of miR223 from mitochondria. Cytosolic miR223 is
968 enriched in mitochondria where it may be sequestered by a weak

interaction with YBAP1. Cytoplasmic YBX1 interacts more tightly with miR223 which may drive the removal of miR223 from mitochondria. YBX1 in RNA granules may accumulate miR223 removed from mitochondria. YBX1 puncta may give rise to small particles carrying miR223 for uptake into endosomes and secretion in exosomes.

Figure 1 – source data. Uncropped gel images corresponding to Figure 1.

Figure 1 – figure supplement 1 – source data. Uncropped gel images corresponding to Figure 1 supplement 1.

Figure 2 – source data. Uncropped gel images corresponding to Figure 2.

Figure 2 – figure supplement 1 – source data. Uncropped gel images corresponding to Figure 2 supplement 1.

Figure 3 – source data. Uncropped immunoblot images corresponding to Figure 3.

Figure 3 – figure supplement 1 – source data. Uncropped immunoblot images corresponding to Figure 3 supplement 1.

Figure 4 – source data. Uncropped immunoblot and gel images corresponding to Figure 4.

Figure 4 – figure supplement 1 – source data. Uncropped gel images corresponding to Figure 4 supplement 1.

Figure 4 – figure supplement 2 – source data. Uncropped gel images corresponding to Figure 4 supplement 2.

Figure 5 – source data. Uncropped immunoblot images corresponding to Figure 5.

Figure 1. YBX1 directly and specifically binds miR223

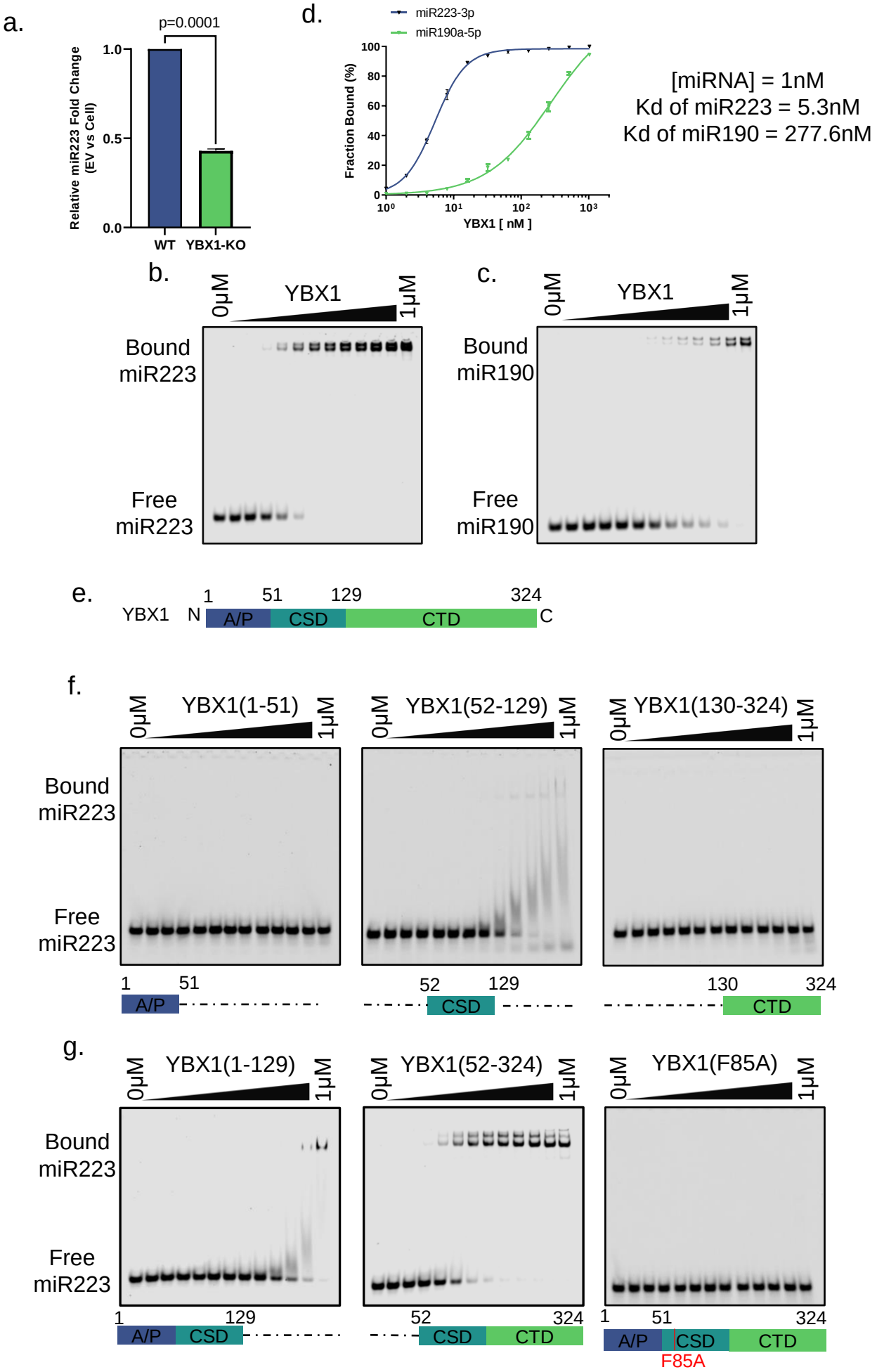

Figure 1-figure supplement 1. Purification of YBX1 full length protein and different truncations and mutation

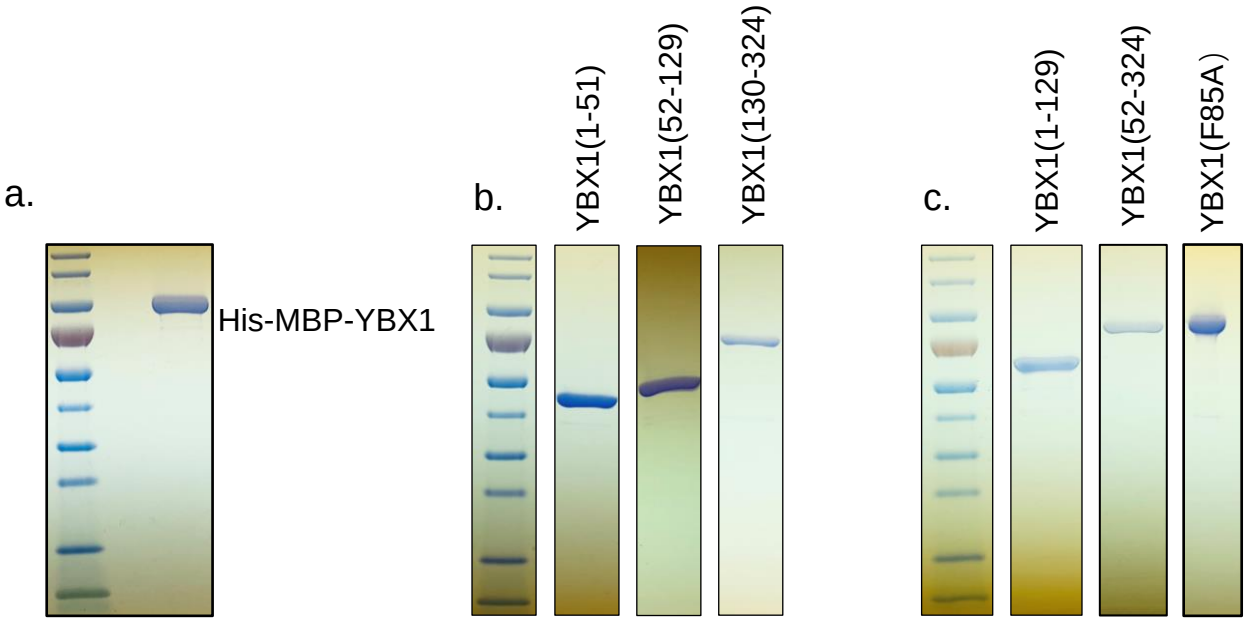

Figure 2. miR223 sequence motif UCAGU binds YBX1

a.

miR223-3p	UG**UCAGU**UUGUCAAAUACCCCA
miR223mut	UG**AGACA**UUGUCAAAUACCCCA
miR190-5p	UG**AUAUG**UUUGAUAUAUUAGGU
miR190sort	UG**UCAGU**UUUGAUAUAUUAGGU

c.

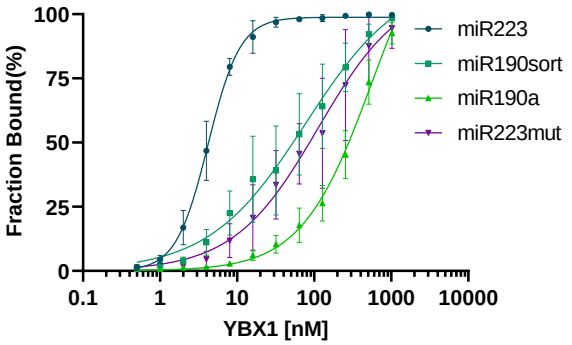

b.

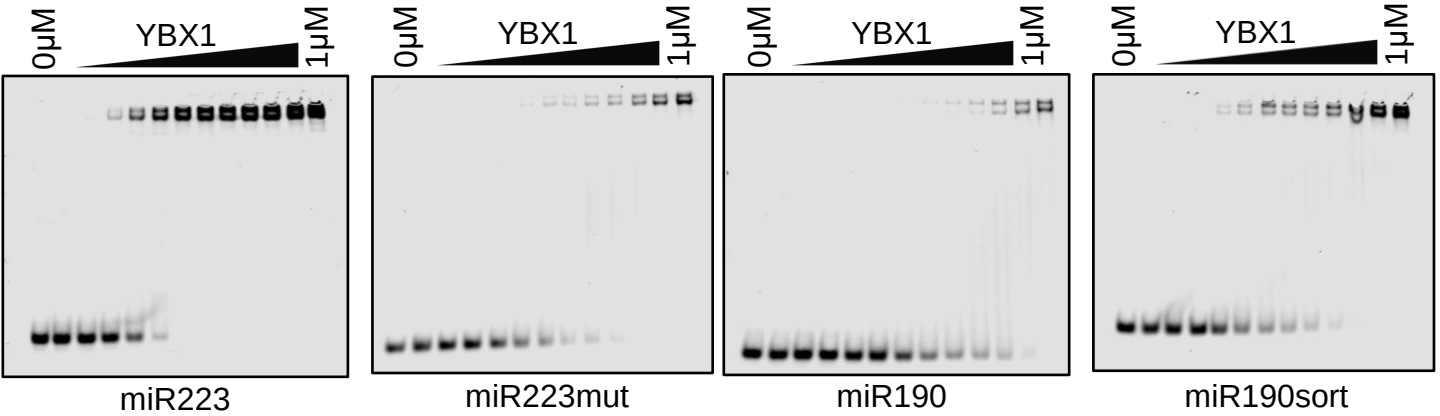

d.

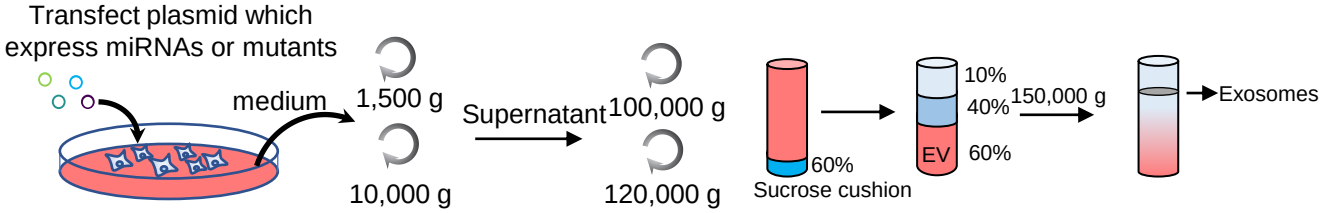

e.

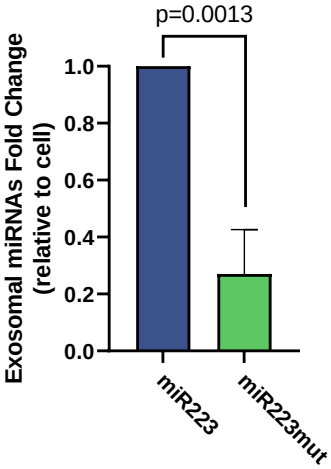

g.

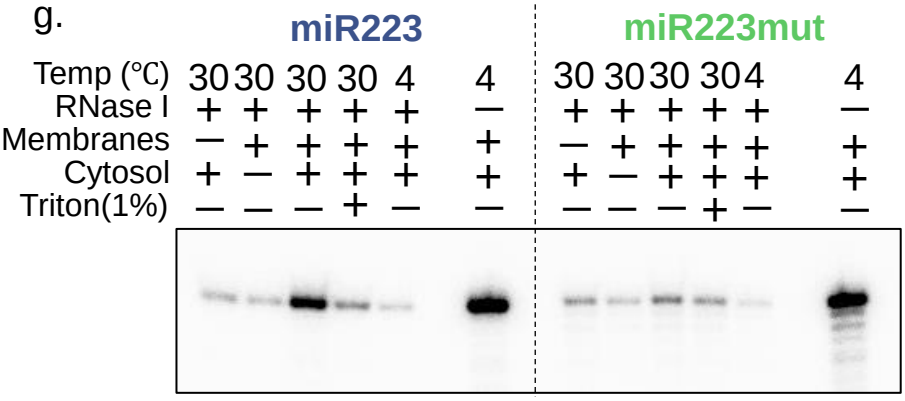

f.

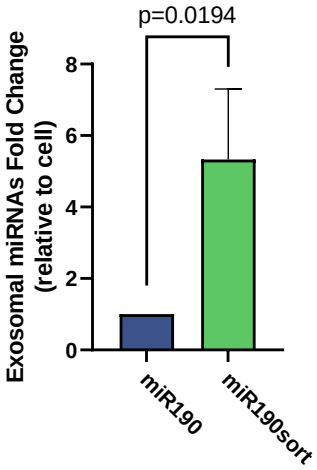

h.

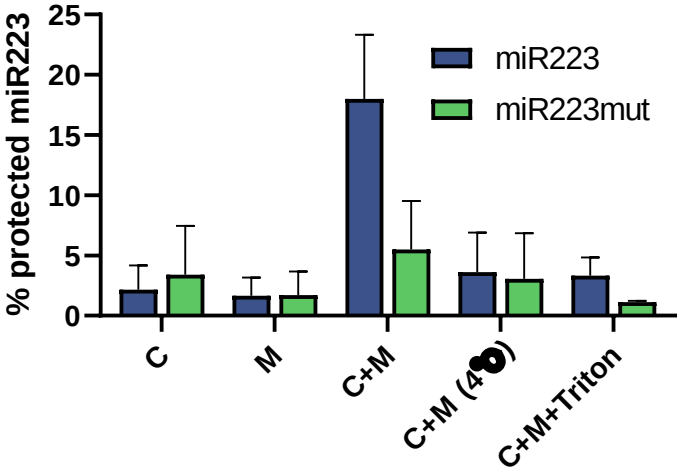

Figure 2-figure supplement 1. Screening exosomal sorting motif of miR223

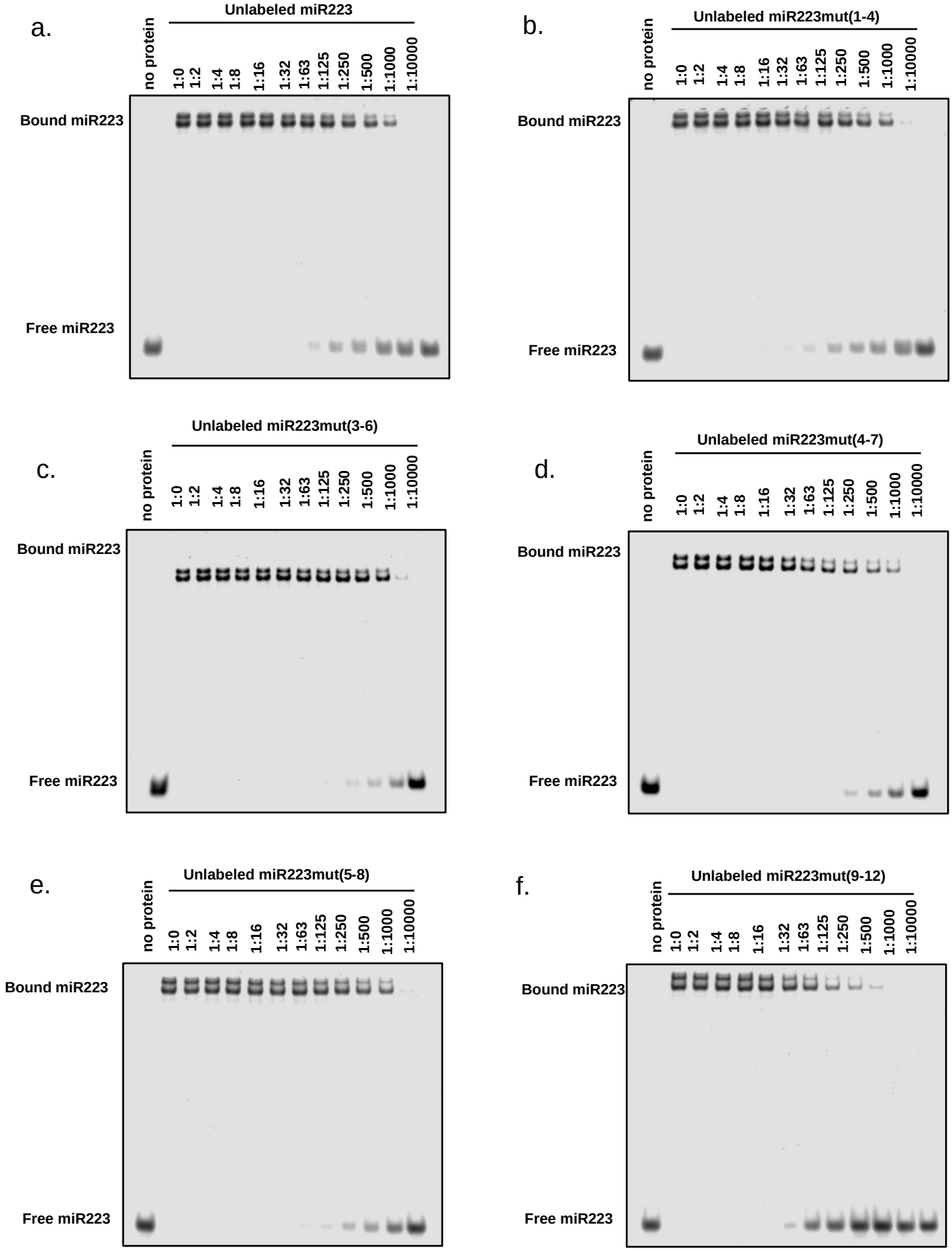

Figure 3. Mitochondria contribute to miR223 enrichment into exosomes

a.

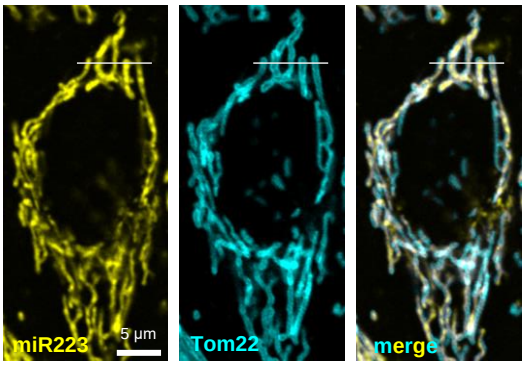

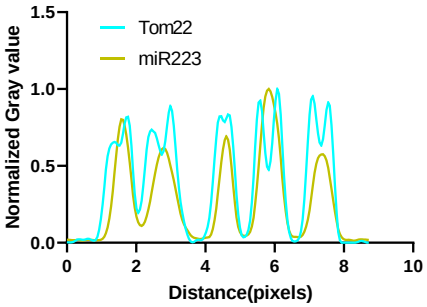

b.

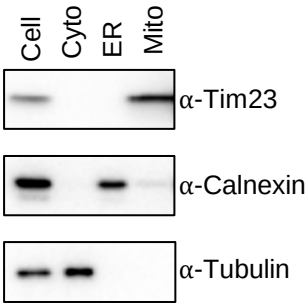

c.

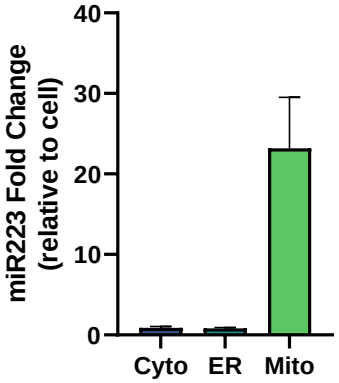

d.

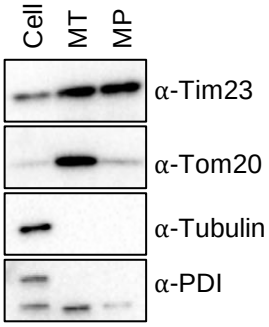

e.

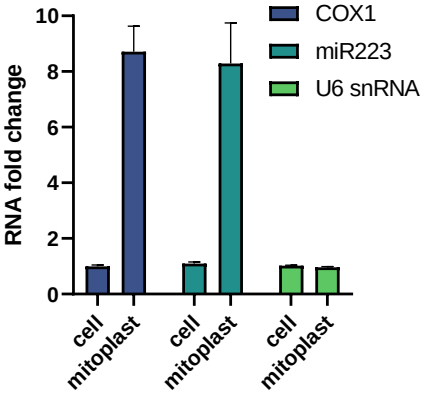

f.

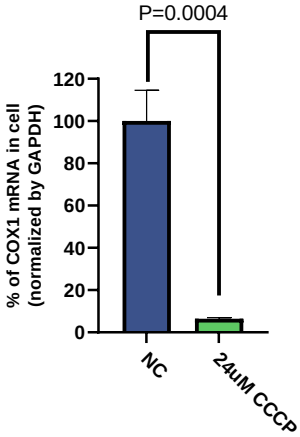

g.

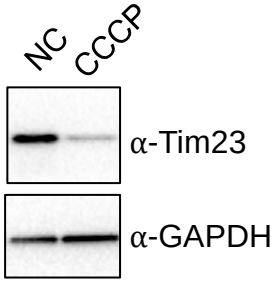

h.

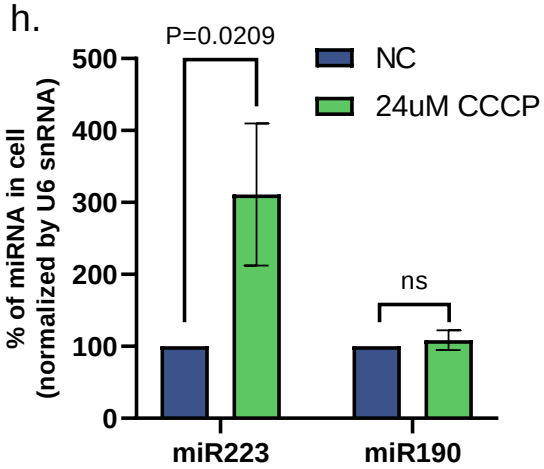

i.

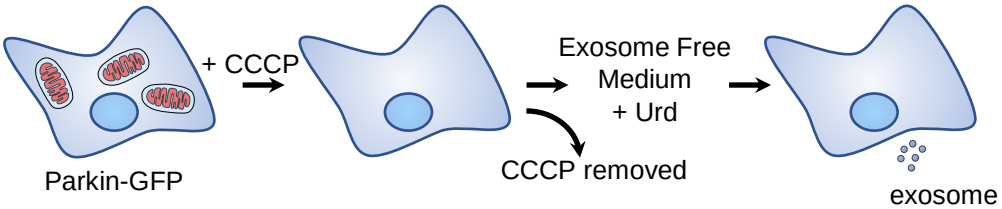

j.

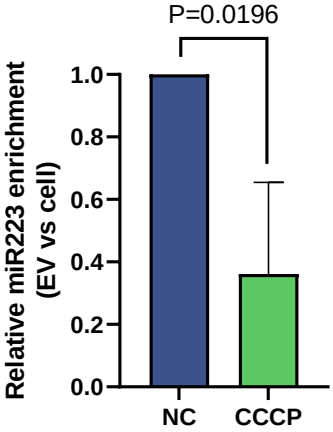

Figure 3-figure supplement 1. miR223, but not miR190, enriched in mitochondria.

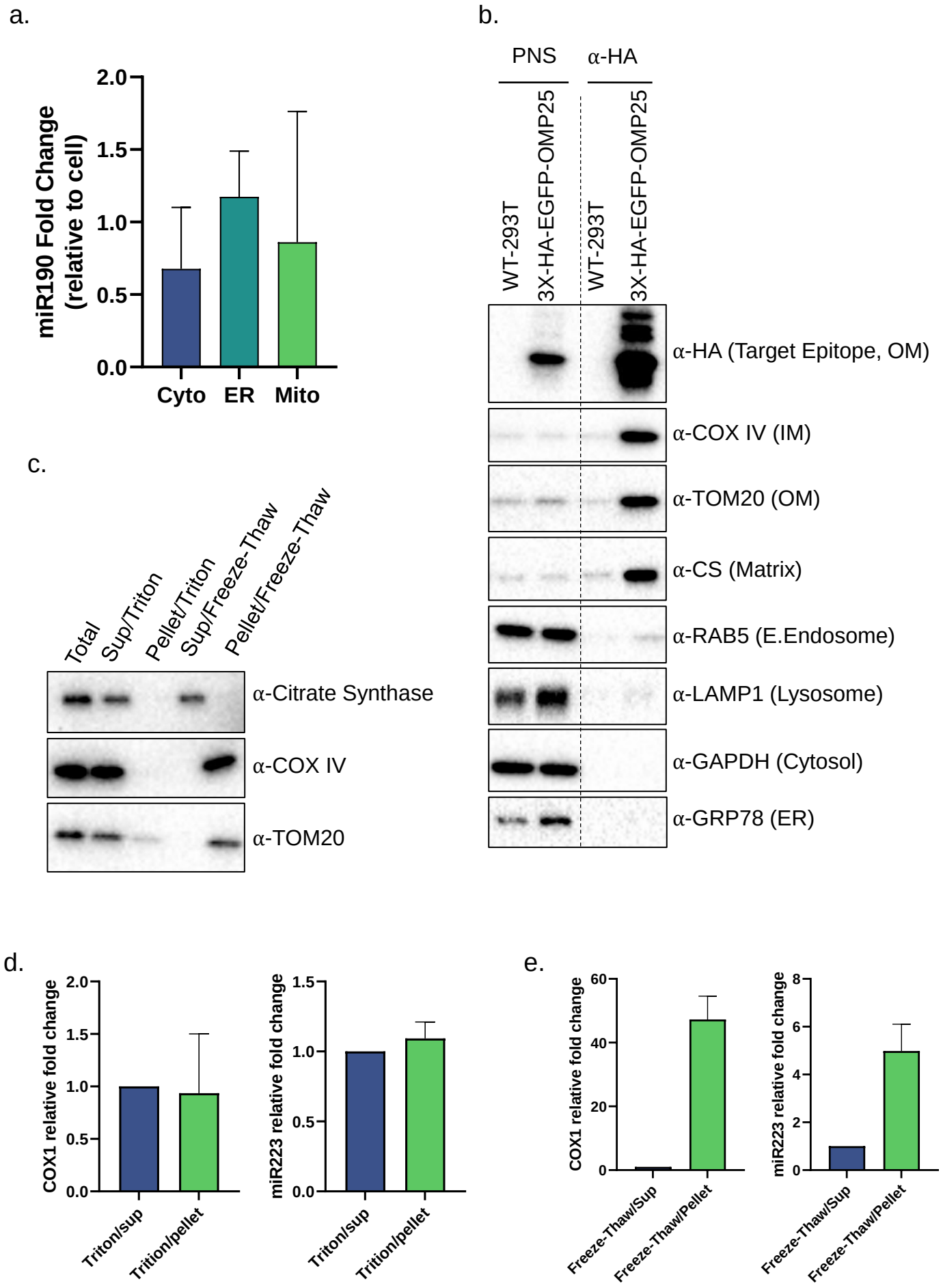

Figure 4. YBAP1 binds miR223 in the mitochondria and in vitro

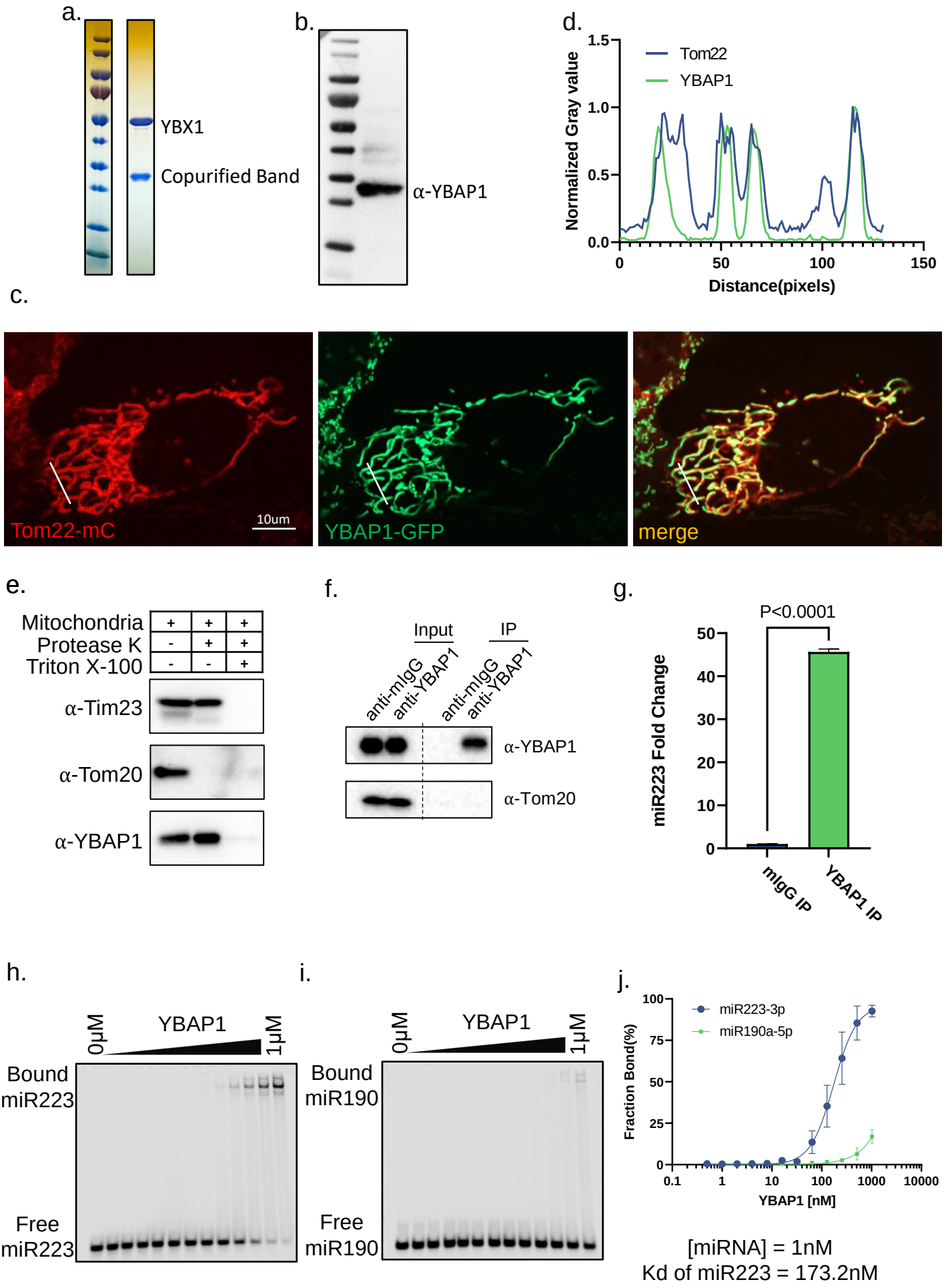

Figure 4-figure supplement 1. YBX1 and YBAP1 copurify as a complex from transfected SF9 cells.

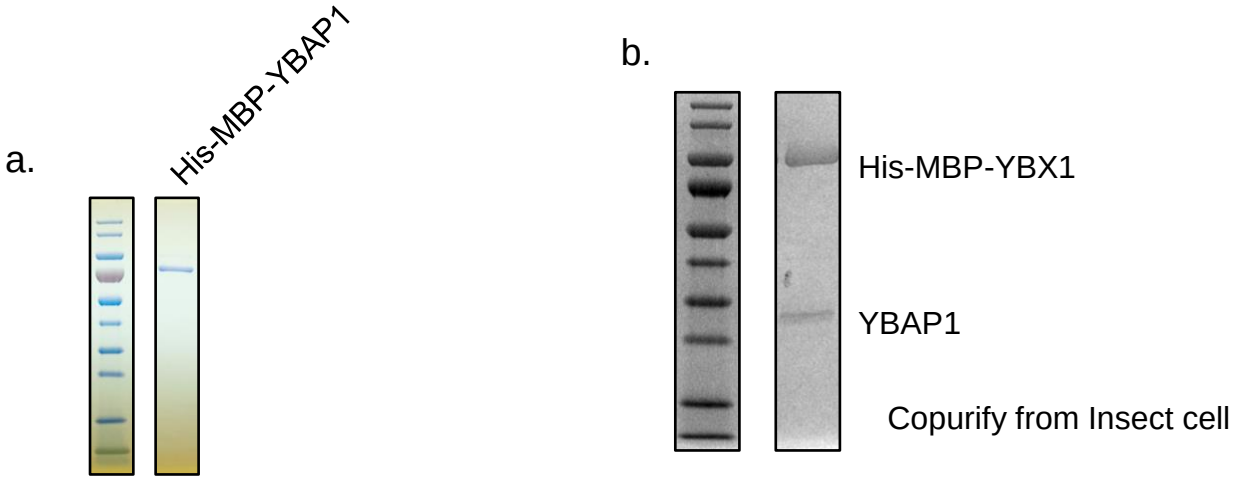

Figure 4-figure supplement 2. YBAP1 does not share the same motif as YBX1 that binds to miR223

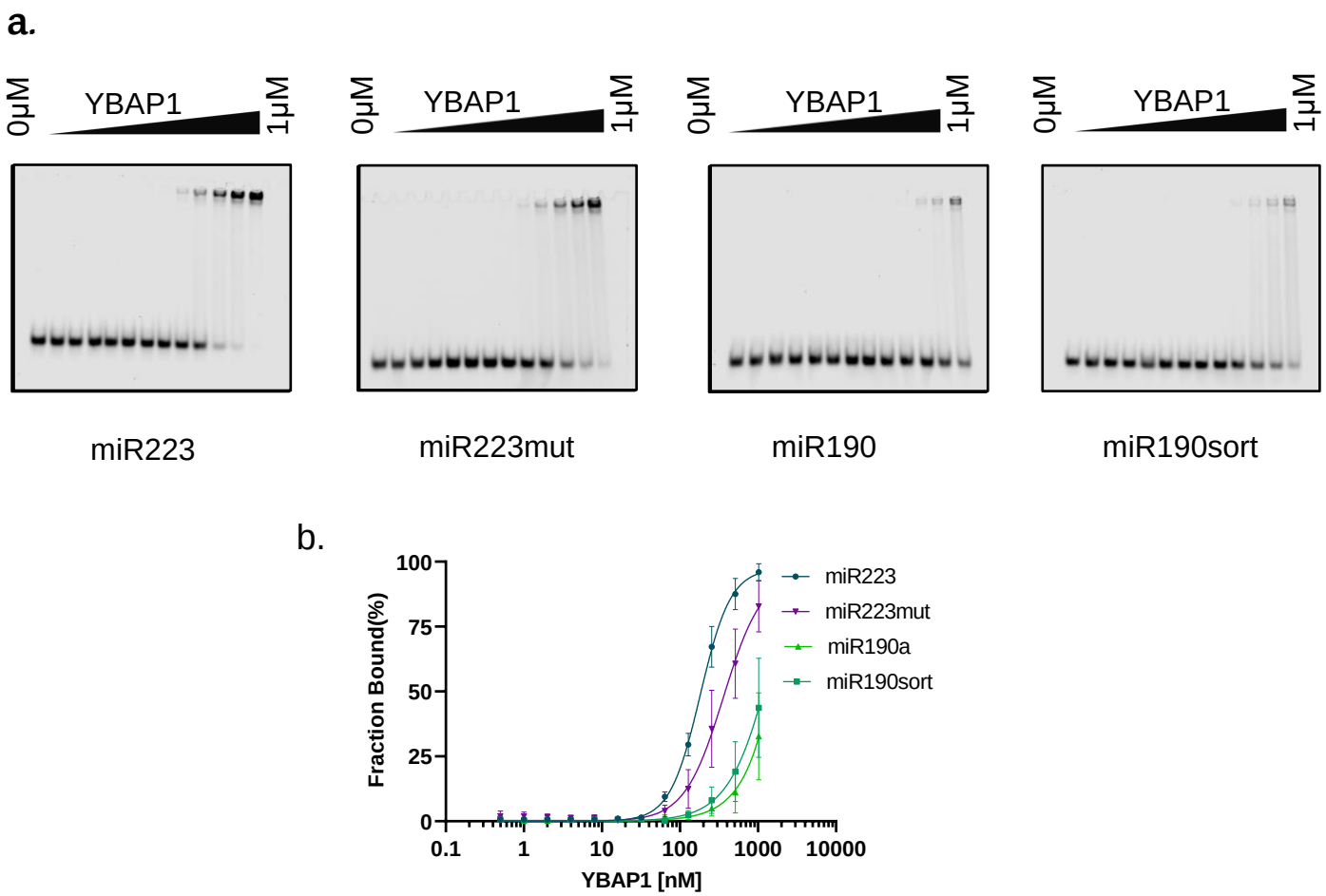

Figure 5 . YBAP1 sequesters miR223 which is released and secreted in YBAP1 KO cells

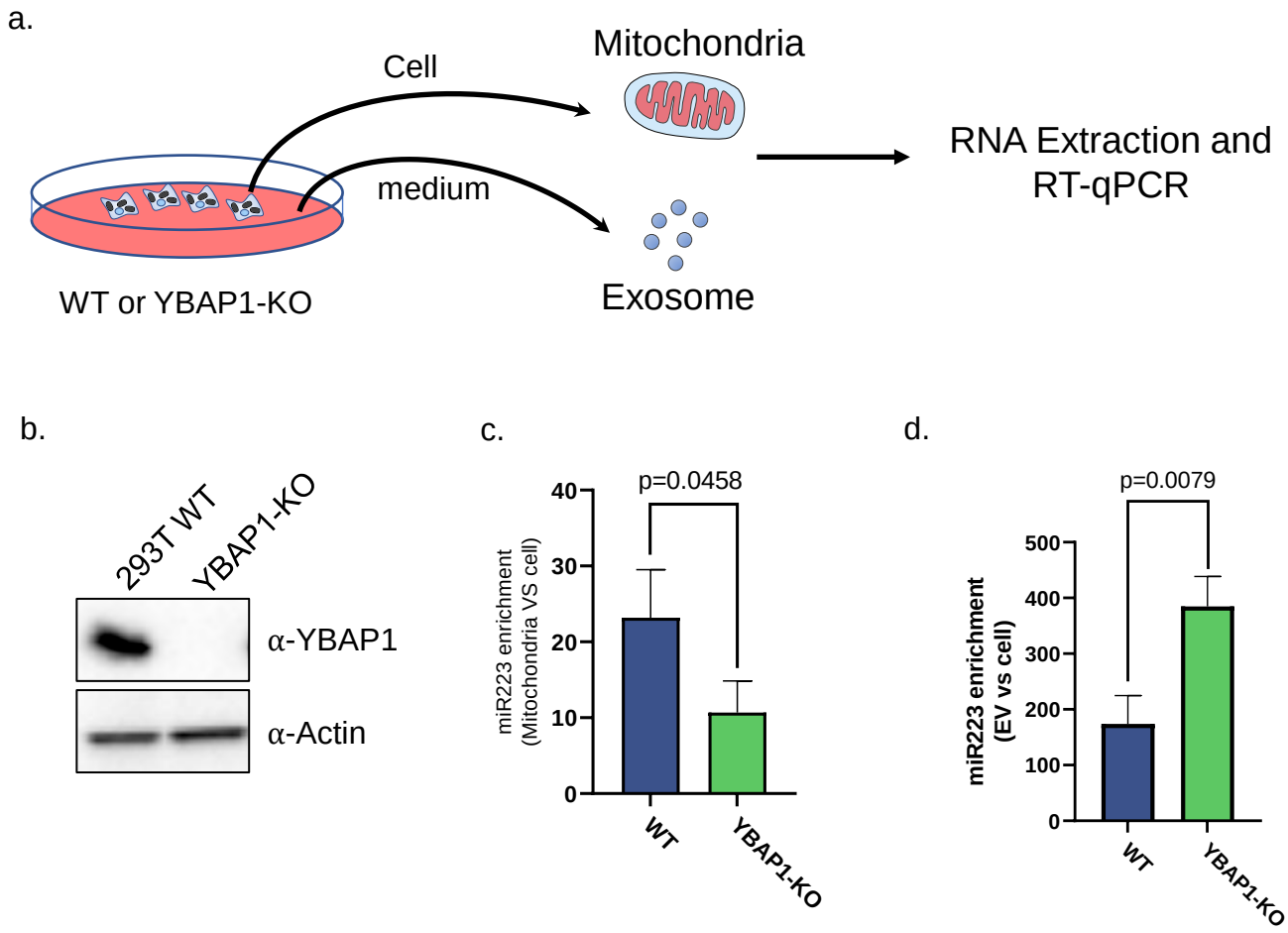

Figure 6. YBX1 puncta relocalize from mitochondria to endosomes

a.

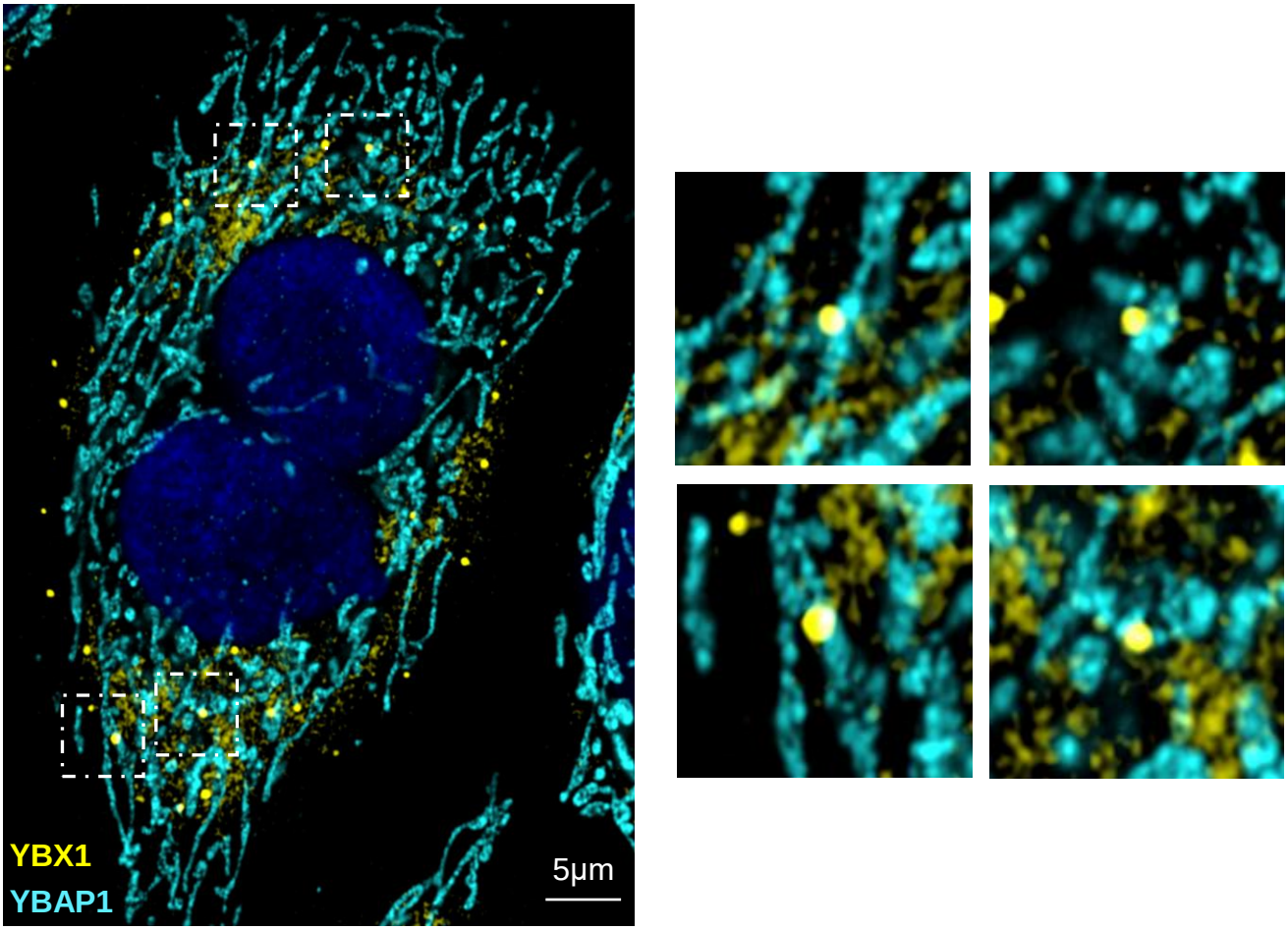

b.

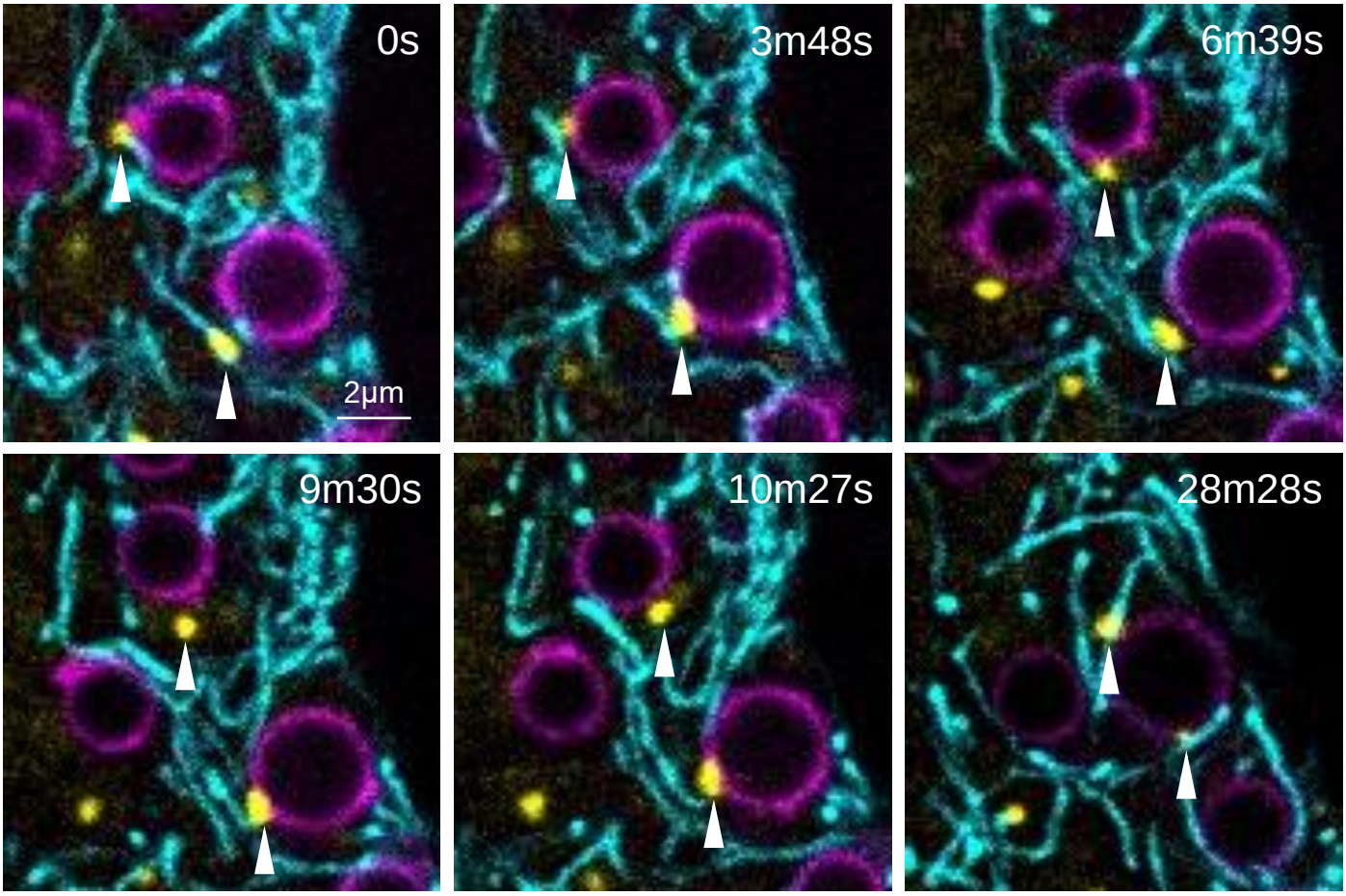
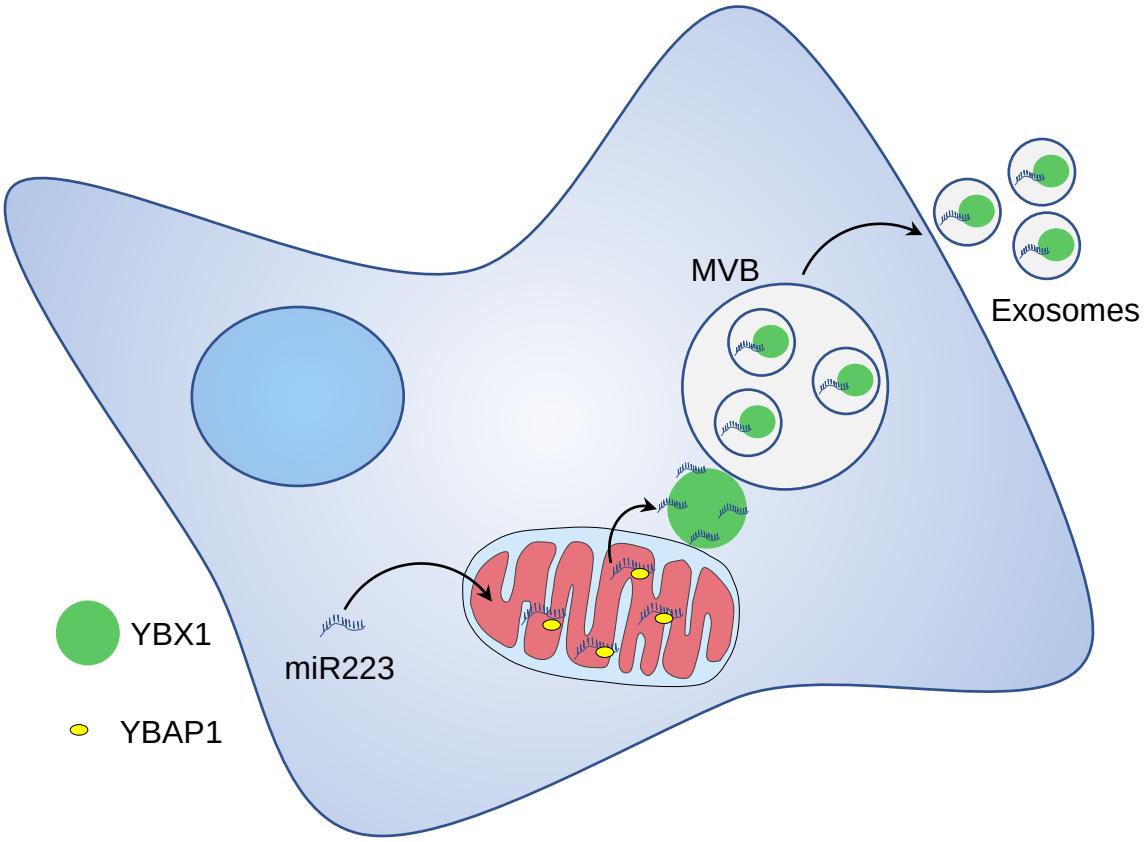
Figure 7. Diagram representing a model of miR223 sorting from mitochondria into exosomes